Establishment of a psoriatic skin model for radon treatment*

J. Wiedemann[1], *C. L. Witzler*[1], *M. Kovacs*[2], *M. Podda*[2], *and C. Fournier*[1,3]
[1]GSI, Darmstadt, Germany; [2]Department of Dermatology, Darmstadt Hospital; [3]Hochschule Darmstadt, Germany

Introduction

Psoriasis is a common chronic inflammatory skin disease [1] which is on the indication list for the therapy in radon galleries [2], but the mechanisms underlying the clinical benefit are still unclear. The disease is characterized by red plaques with white scales at elbows, knees and scalp and triggered by many factors like injury and trauma. In general it is due to an overshooting and persisting activation of the immune system. For the manifestation IL-17, IL-22, TNF-α and IFN-γ released from Th17, Th1 and Th22 cells are essential to contribute to the inflammatory cytokine milieu and to trigger an amplifying feedback loop, which is responsible for the pathogenesis [3, 4].
The access to skin biopsies from psoriasis patients and patients treated in radon galleries is limited. Therefor a model system which is close to the in vivo situation is needed for radon exposure experiments (Figure 1).

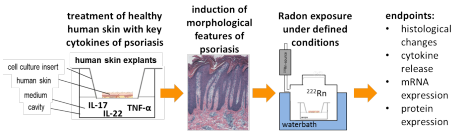

Figure 1: Experimental setup for induction of a psoriatic skin model and exposure in the radon chamber [5]

Material and Methods

Human skin from surgeries (FF136/2014) is cultured as explant at the air liquid interface (ALI) and treated with IL-22, IL-17 and TNF-α (100 ng/ml) alone or in combination for 24 or 48 hours. Then the samples are prepared for histology, immunostainings and qPCR; medium is collected for cytokine analysis. A H&E staining and an antibody staining of Psoriasin and Keratin 16 is performed.

Results and Discussion

Hematoxylin & Eosin staining of human skin treated with key cytokines of psoriasis (Figure 2) shows parakeratosis, an unsharp connection between stratum granulosum and stratum corneum and an impaired tissue organisation [6]. Immunostaining of Psoriasin (S100A7) (Figure 3) revealed a slight expression in controls and an enhancement after treatment with IL-22 or IL-17. A combined treatment with IL-22, IL-17 and TNF-α shows a synergetic effect. These results show that treatment with IL-17, IL-22 or a combination of IL-17, IL-22 and TNF-α can induce an impaired differentiation and an enhanced expression of Keratin 16 and Psoriasin which are key markers of Psoriasis. These are first hints to a successful induction of psoriatic features.

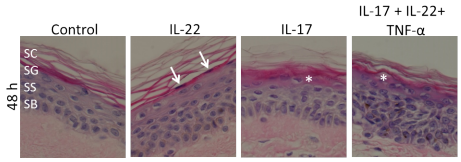

Figure 2: H & E staining of human skin explants 48 h after treatment with IL-22, IL-17 or a combination of IL-22, Il-17 and TNF-α; arrows mark parakeratosis, stars mark the unsharp connection between SG and SC

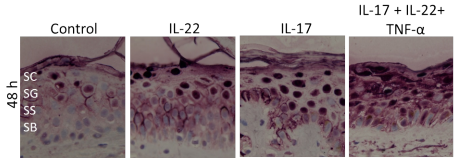

Figure 3: Psoriasin (S100A7) staining of human skin explants 48 h after treatment

*Work supported by Forschungsinstitut Bad Gastein (FOI-15/08-031WIE), EURADON, the Radon Gallery of Bad Gastein and GREWIS (02NUK017A)

References

[1] Lowes MA et al.; Nature (2007) 445:866–73. doi:10.1038/nature05663
[2] Gasteiner Kur- Reha- und Heilstollen Betriebsges.m.b.H. Indikationen; www.gasteiner-heilstollen.com
[3] Johnson-Huang LM et al.; Dis Model Mech (2012) 5:423–33. doi:10.1242/dmm.009092
[4] Chu C-C et al.; Semin Immunol (2011) 23:28–41. doi:10.1016/j.smim.2011.01.006
[5] Maier A et al.; Nucl.Instrum.Meth.(2015); 362, 187-193; doi10.1016/j.nimb.2015.09.042
[6] Simoniello P. et al.; Front. Oncol. (2015) 5:294.; doi: 10.3389/fonc.2015.00294

Contribution of radon decay products to lung dose*

A. Maier[1], *S. Sternkopf*[1,2], *H. Schmidt-Böcking*[2], *G. Kraft*[1], *C. Fournier*[1]
[1]GSI, Darmstadt, Germany; [2]Goethe Universität Frankfurt a. M., Germany

Introduction

Radon is one of the main contributors to annual dose from natural sources. Additionally radon exposure is associated with an increased risk for lung cancer [1]. The lung dose arises from radon and its decay products that can be attached to aerosols. The formation of radioactive aerosols is shown in figure 1. The radon decay products can react with vapour and form unattached progeny. Subsequently they can form clusters with dust particles (attached progeny). The deposition mechanism depends on the size of the aerosols but will not be investigated in this work. In this study we want to quantify the contribution of the radon decay products to the lung dose in relation to the radon concentration and independent from the size of the particle.

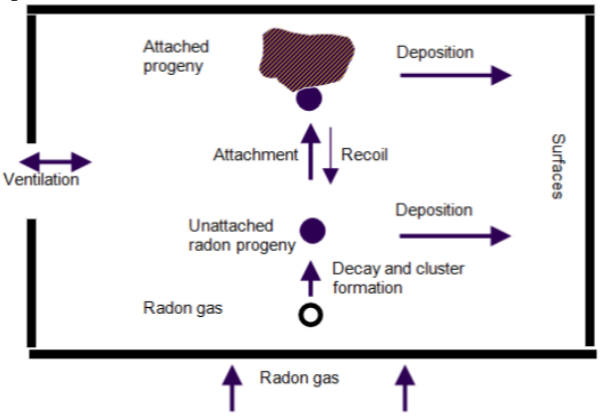

Figure 1: Formation of radioactive aerosols [2]

Measurement setup

For the experiments we developed a mechanical lung model (see figure 2). The radon progeny are deposited on a glas fibre filter and radon is absorbed on activated coal, both inside a small tube. The flow through the model is regulated by a pump and measured by a flow-meter. The whole setup is placed in a big radon chamber. For variation of the aerosol concentration we changed the relative humidity in the measurement setup.

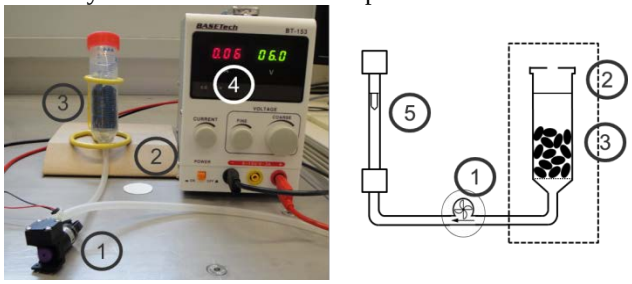

Fig. 2: Overview of the lung model with: 1 pump, 2 filter, 3 tube with activated coal, 4 power supply, 5 flowmeter

After exposure the activity of the decay products and radon were determined by gamma- spectroscopic measurements and the dose caused by the attached aerosols was determined as function of humidity [3].

Results

The results of our first measurements are shown in figure 3 where we plotted the dose of the filter over the relative humidity during the experiments. The results are normalised to a radon concentration inside the big radon chamber of 400 kBq/m^3. With these measurements we could show the feasibility of our method. But the scatter of the data points is too large to identify a clear increase.

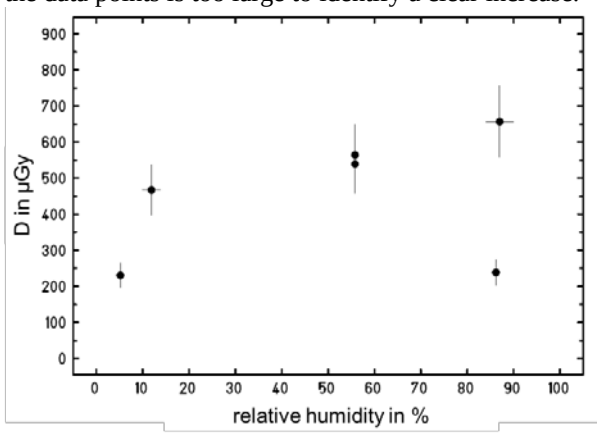

Fig. 3: Calculated dose from radon progeny in dependence of the relative humidity [3]

Outlook

For future work there are several improvements of the measurement setup. Amongst others we want to construct a more anatomical correct lung model and a reproducible variation of the aerosol concentration. In combination with a certain size distribution of the aerosols, the deposition mechanism at different sites in the lung can be investigated.

References

[1] S. Darby et al. Residential radon and lung cancer – detailed results of a collaborative analysis of individual data on 7148 persons with lung cancer and 14208 persons without lung cancer from 13 epidemiologic studies in Europe, Scand. J. Work Environ. Health, 32, 1-84, 2006

[2] Committee on Health Risks of Exposure to Radon, National Research Council, Health Effects of Exposure to Radon (BEIR VI), National Academy Press, 1999

[3] S. Sternkopf, Dosisbeitrag von Radonzerfallsprodukten in der Lunge, Bachelor Thesis, Goethe University, Frankfurt, 2016

* Work is supported by BMBF project funding reference number 02NUK017A

DOI:10.15120/GR-2017-1

Towards the multi-ion treatment planning with ^{16}O beams

O. Sokol[*1], *E. Scifoni*[2], *S. Hild*[2], *M. Durante*[2], *and M. Krämer*[1]

[1]GSI, Helmholtz Centre for Heavy Ion Research, Darmstadt, Germany; [2]TIFPA Trento Institute for Fundamental Physics and Applications, Trento, Italy

It was recently demonstrated theoretically and experimentally [1] that ^{16}O ions might be able to produce lower damage to residual tissue in several cases of hypoxic (with partial oxygen pressure $pO_2 < 21\%$) tumors irradiation. Meanwhile, the cell kill in the normally oxygenated regions ($pO_2 = 21\%$) is expected to be higher due to the increased LET and, consequently, RBE values of ^{16}O. These two statements allow one to expect further dose decrease for the residual tissue when combining light and heavy ion modalities inside one plan, e.g. by forwarding high-LET ^{16}O ions only to the hypoxic parts of the target, while covering the rest with lighter particles (p, ^{4}He).

TRiP-98 multiion

The current 'mainstream' version of GSI in-house treatment planning system TRiP98 allows including several ion modalities inside one plan. Another 'proof-of-concept' version TRiP98-OER [2, 3] accounts for tumor hypoxia by means of kill-painting approach, but only for single-ion fields. In order to test the hypothesis mentioned above, TRiP98 was expanded by merging these two versions.

^{16}O + ^{4}He combined planning

Figure 1 describes the geometry of the test treatment plan. The target of 40×40×60 mm with hypoxic (pO_2 = 0.15%) central region of 28 mm was placed at 80 mm depth inside the 160 mm CT cube. The RBE tables for CHO cells [1] with α/β = 11 were used for the calculations of biological effects with LEM IV. Figure 2 represents the tests of plans optimized for a uniform target survival level of 10%. Three cases were analyzed: single-ion optimizations with opposite ^{4}He or ^{16}O fields, and quadruple-field optimization with two pairs of opposite fields (^{16}O + ^{16}O and ^{4}He + ^{4}He).

Table 1 shows the corresponding survival values in the entrance channel (EC) region at depths of 5 mm (beam entrance) and 45 mm (target border region). For the combined plan ^{16}O + ^{4}He these values are the highest with the same damage to the target. At 5 mm depth the relative increase of EC survival will be 12.1% and 19.6% compared to pure ^{16}O and pure ^{4}He irradiations, accordingly. At a higher depth of 45 mm the difference increases towards 26.8% and 34.6%, accordingly.

Revealing the conditions for the highest benefit from applying this method, and its experimental verification are subjects of further investigation.

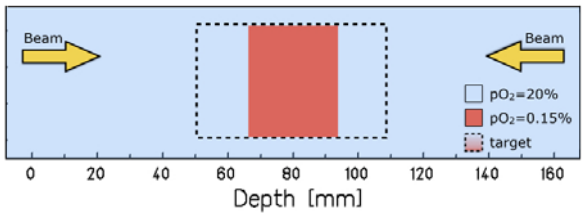

Figure 1: Geometry, oxygenation distribution and fields directions for the test plan. Target borders are marked with a dashed line.

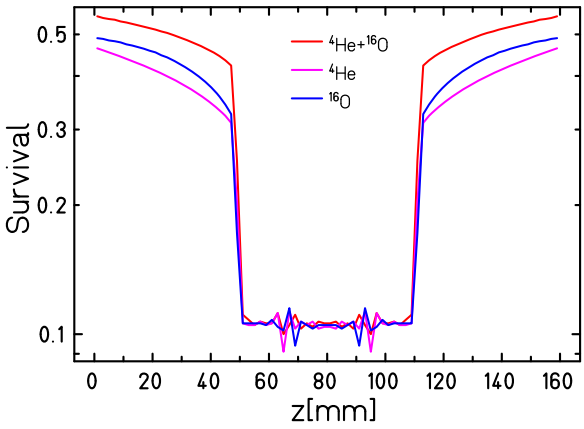

Figure 2: Survival distribution for single-ion double-field optimizations (^{4}He + ^{4}He and ^{16}O + ^{16}O), and multiion quadruple-field optimization (^{16}O + ^{16}O + ^{4}He + ^{4}He).

Depth (mm)	EC survival, %		
	O	He	O+He
5	48.4	45.4	54.3
45	34.3	32.3	43.5

Table 1: Numerical values of EC survival at different depth for three cases of irradiation shown in Figure 2.

References

[1] O. Sokol et al, submitted to Phys. Med. Biol.

[2] Scifoni et al, Including oxygen enhancement ratio in ion beam treatment planning: model implementation and experimental verification, Phys. Med. Biol. 58 (2013)

[3] W. Tinganelli et al, Kill-painting of hypoxic tumours in charged particle therapy, Sci. Rep. 5 (2015).

* o.sokol@gsi.de

Influence of Poly(ADP)ribosylation on radiation-induced chromatin decondensation

A. Heselich[1], L. Pack[1], G. Taucher-Scholz[1,2] and B. Jakob[1]
[1]GSI, Darmstadt, Germany; [2] TU Darmstadt, Darmstadt, Germany

Motivation

Aim of our project is the identification of factors responsible for the observed chromatin changes in proximity of heavy ion induced clustered lesions [1]. First we focussed on Heterochromatin protein 1 (HP1), which showed no significant influence on the condensation and relocation of heterochromatic damages after targeted irradiation of mammalian cells [2]. This finding was in contrast to data published using *Drosophila* cells [3], but goes in line with very recent publications using CRISPR/Cas9-mediated heterochromatic (HC) DNA DSB induction [4]. New publications using UV laser micro-irradiation have recently shown that inhibition of the repair factor PARP1 has a significant influence on chromatin expansion [5]. Since this is a first indication that PARP1, possibly via its PARylation activity, could also play a role in chromatin decompaction at complex damages we started to analyse the effect of PARP inhibition on chromatin decondensation after heavy ion irradiation.

Materials & Methods

Murine fibroblasts (NIH/3T3) or U2OS-NBS1-GFP2 were treated with PARP inhibitor PJ34 prior to DNA damage induction. Inhibitor efficiency was checked via PAR staining after treatment with H_2O_2 as positive control. U2OS-NBS1-GFP2 cells were stained with Hoechst 33342 and irradiated with a 337 nm UV-laser to analyse the influence of PARPi on chromatin expansion and at the same time to check for accumulation of GFP-tagged NBS1 to verify efficient DNA-DSB induction. NIH/3T3 cells were irradiated with Helium ions (76 keV/µm) at the UNILAC accelerator and decondensation of heterochromatin at DNA-DSBs was evaluated 5 min post IR.

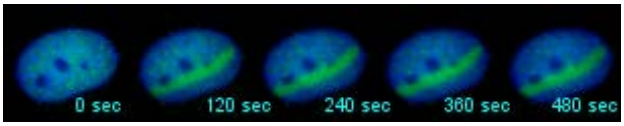

Figure 1: Laser irradiation showed efficient DNA-DSB induction in U2OS-NBS1-GFP2 as verified via NBS1 recruitment (green = NBS1; blue = DNA).

Results

First we verified that PARP1 inhibition was able to influence the chromatin expansion after DNA-DSB induction via laser irradiation under the applied conditions (Fig. 1,2). PARPi treated U2OS showed a reduced chromatin expansion compared to control cells (Fig 2). In preliminary experiments using Helium ion irradiation the vast majority of HC areas traversed by He ions still showed a signature of radiation induced decondensation. We could only find tendency of slightly increased number of chromocenters showing no decondensation at the DNA damage site in PARPi treated NIH/3T3 cells (Fig. 3). This is in contrast to the general inhibition of chromatin opening in the UV-laser experiments using PARP inhibition.

Summary

We could show an influence of PARP1 activity on chromatin decondensation after DSB-induction after UV-laser irradiation, which was hardly visible after ion irradiation. It is possible that different remodelling factors are predominatly used for lesion of different complexity.

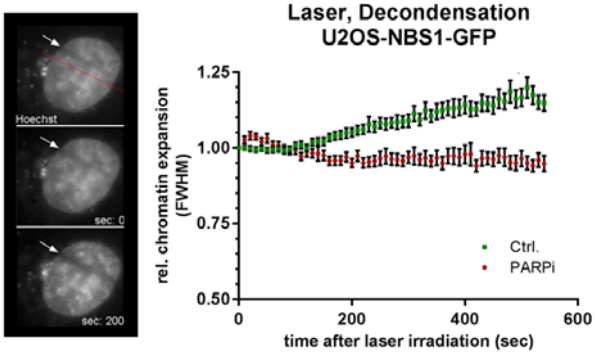

Figure 2: Decondensation measured via chromatin expansion showed an inhibited expansion in U2OS cells treated with PARPi (PJ34, 10µM). Left panel shows an example of chromatin expansion after laser irradiation over time. Right panel represents analysis (FWHM) of relative chromatin expansion (mean±SEM, n ≥45 nuclei).

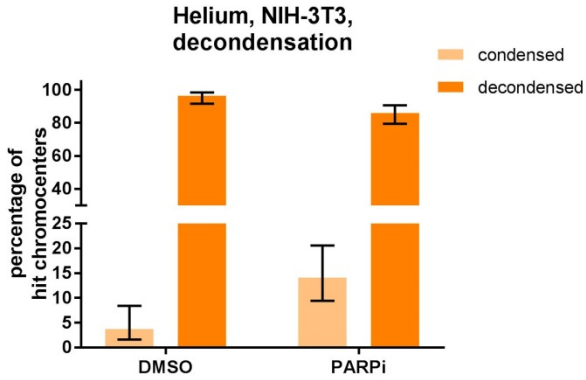

Figure 3: PARPi treated NIH/3T3 cells show a tendency to less decondensed chromocenters (CC) after heavy ion irradiation (He, 76 keV/µm). Data represent percentage of hit CC (n ≥ 135 CC) 5 min post irradiation, error bars represent 95% confidence interval based on binomial distribution.

References

1. Jakob, B., *et al.* NAR **39**, 2011.
2. Heselich, A., *et al.* Scientific Report, 2015.
3. Chiolo, I., *et al.* Cell **144**, 2011.
4. Tsouroula, K., *et al.* Mol Cell **63**, 2016.
5. Strickfaden, H., *et al.* J Biol Chem **291**, 2016.

We thank C. Lukas (University of Copenhagen) for kindly providing the U2OS-NBS1-GFP2- cells.
This work is supported by the German federal ministry of education and research (BMBF). Grant#: 02NUK037A.

DOI:10.15120/GR-2017-1

Measurement of neutron production by high energy protons in space radiation shielding materials

F. Horst[*1,2], *C. Schuy*[1], *M. Rovituso*[3], *M. Giraudo*[4], *K. Zink*[2], *and U.Weber*[1]

[1]GSI, Darmstadt, Germany; [2]THM, Giessen, Germany; [3]TIFPA, Trento, Italy; [4]Thales Alenia Space, Turin, Italy

Introduction

An experiment was carried out at the Trento proton therapy center within the ROSSINI-2 project funded by ESA [1]. The aim of this experiment was to measure and to compare the neutron production by high energy protons in different space radiation shielding materials (LiH, moon concrete, polyethylene, aluminum).

Methods and Materials

Targets of the different materials were irradiated with $228\ \mathrm{MeV}$ protons delivered at high intensities ($100\ \mathrm{nA}$ cyclotron current) with at least 10^{12} protons per measurement. Three passive dosimeters, usually applied for radiation monitoring at GSI [2] were used for the measurements. They consist of a TLD cartridge (two TLD600H chips sensitive to photons and thermal neutrons and two TLD700H chips only sensitive to photons) inside a polyethylene moderator with a lead layer. They were placed at $15\,°$, $65°$ and $90°$ at a distance of $1\ \mathrm{m}$ from the target. A $21 \times 21\ \mathrm{cm}^2$ air-filled parallel plate ionization chamber was used to monitor the proton fluence. After traversing the targets, the protons were stopped within a water beam dump. For every material three different target thicknesses were irradiated. The experimental setup is illustrated in Figure 1.

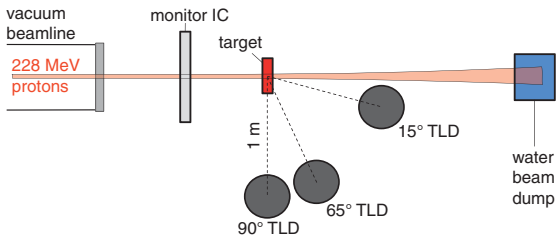

Figure 1: Experimental setup used at the Trento proton therapy center to measure neutron production in different space radiation shielding materials.

All TLDs were individually calibrated beforehand using a $^{137}\mathrm{Cs}$ source for absorbed dose and the conversion factor to neutron ambient dose equivalent was obtained by calibration measurements with an $^{241}\mathrm{AmBe}$ neutron source. The TLDs were readout within 3 days after irradiation using an automated TLD reader (Harshaw 6600 Plus Automated TLD reader) and corrected for background dose using four unirradiated cartridges. The neutron dose originating from the water beam dump (see experimental setup in Figure 1) was measured in a no-target run and was appropriately subtracted from the target-in measurements. The neutron ambient dose equivalent was then calculated by averaging the two TLD-600H readings (neutron + photon dose), subtracting the average of the two TLD-700H readings (only photon dose) per cartridge and applying the conversion factor obtained at the $^{241}\mathrm{AmBe}$ neutron source. The summed relative standard deviation of each averaged dose reading was used as estimated experimental error.

Results

Figure 2 shows exemplary the dataset obtained for the moon concrete targets, in particular the measured neutron ambient dose equivalent $\mathrm{H}^*(10)_n$ in $1\ \mathrm{m}$ as a function of the angle to the beam axis for three different thicknesses. The given neutron dose values are normalized per 10^{12} primary protons striking the target as obtained from the charge reading of the monitor ionization chamber.

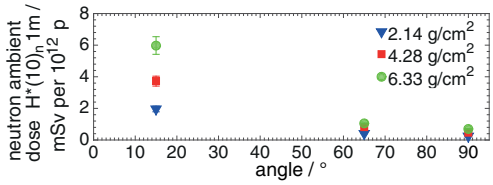

Figure 2: Neutron ambient dose $\mathrm{H}^*(10)_n$ in $1\ \mathrm{m}$ at $15°$, $65°$ and $90°$ generated by $228\ \mathrm{MeV}$ protons in moon concrete measured for three different target thicknesses.

As expected, the generated neutron dose is roughly proportional to the thickness of the irradiated target. The angular dependence shows that there is a forward trend in the emission direction of the neutrons.
Further work will be done to compare the measured neutron production within the different materials together with predictions by different Monte Carlo codes.

References

[1] C. Schuy, M. Rovituso, R. Pleskac, C. La Tessa, M. Durante "The ROSSINI project at GSI", GSI Scientific Report 2013 (2014)

[2] G. Fehrenbacher, F. Gutermuth, E. Kozlova, T. Radon and R. Schuetz "Neutron dose measurements with the GSI ball at high-energy accelerators", Rad. Prot. Dos. 125 (2007)

* f.horst@gsi.de

Commissioning of the MIMOSA28 for radiotherapy application

C.-A. Reidel[1,2], *C. Schuy*[1], *Ch. Finck*[2], *and U. Weber*[1]
[1]GSI, Darmstadt, Germany; [2]IPHC, Strasbourg, France

Introduction

In radiotherapy, monitoring the deposited dose in a patient is a critical issue. MIMOSA28 – also called ULTIMATE – [1] is used for the tracking of charged particles. With a readout of 185.6 μs and a spatial resolution < 5 μm, MIMOSA28 is a good candidate for online monitoring of the Bragg peak. In this case, the sensor would be placed on the side of the target for the detection of the lighter fragments.

Motivations

The sensors will be used in different places for different experiments with different configurations. Therefore it is important to have a setup relatively easy to build up while maintaining a precise and reproducible mechanical alignment in order to do a good track reconstruction.

The setup is composed of five electronic boards. Around 30 cables have to be connected properly between the boards and the sensors. Since the boards and the cables are not on a fixed support, it is easy to have a wrong connection and to damage the sensors. The sensors are placed in a holder which also has to be optimized to avoid unwanted interactions like nuclear fragmentation.

The positioning of the set of sensors (telescope) is an important step to be able to have a precise analysis. Before track reconstruction of the produced fragments in a target, the sensors need to be aligned using an alignment run at low intensity without target. The alignment of the sensors is done to mitigate mechanical inaccuracies and placement mistakes (Fig.1).

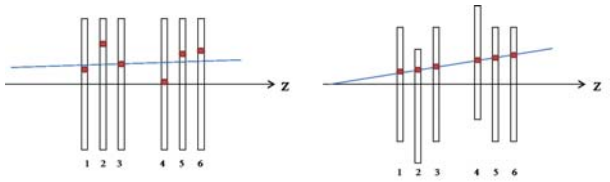

Figure 1: Reconstruction of a track before the alignment (left) and after the alignment procedure (right).

However, the alignment procedure can only be done if the misalignment is smaller than 3° for the rotation for simplifications of the alignment algorithm. It is also important to know the coordinates of the telescope compared to a global system of coordinates. The room where the telescope is placed is then defined as the global system.

Setup optimizations

The first improvement was to build a new holder for the sensor based on an existing design. The main goal of the new holder is to prevent unwanted interactions. Therefore, the holder (made of plastic) has a reduced amount of matter compared to the old design to avoid the interactions between the particle from the beam and the holder which could be detected by the sensor. Moreover, the sensors will be placed on an optical bench to have a good initial position.

Since the setup is intended to be used for different experiments, the optimization of the cabling time needed to be improved. A new box integrating all the 5 boards fixed inside and cabled together has been designed. Around 20 cables are already connected inside the box and the connection to the sensors is relatively fast and easy using feedthrough connectors.

The sensors placed on the optical bench is shown in Figure2.

Figure 2: 6 MIMOSA28 sensors placed the optical bench.

References

[1] Baudot, J. et al., First Test Results Of MIMOSA-26, A Fast CMOS Sensor With Integrated Zero Suppression And Digitized Output.

DOI:10.15120/GR-2017-1

Primary beam attenuation in innovative shielding materials*

C. Schuy[1], F. Horst[1], and U. Weber[1]
[1]GSI, Darmstadt, Germany

Overview

High energetic protons from solar particle events (SPE), HZE ions of the galactic cosmic rays (GCR) as well as trapped particles in the magnetic field of earth pose a serious health risk to astronauts [1]. A possible space radiation mitigation technique is the use of passive shielding [2]. The *ROSSINI2* project (**R**adiati**O**n **S**hielding by I**S**RU and/or **IN**novative mater**I**als for EVA, Vehicle and Habitat) is a common effort of Thales Alenia Space, Trento Institute for Fundamentals Physics Applications, NASA Space Radiation Laboratory, GSI and ESA to select and benchmark the space radiation shielding capabilities of novel materials using ground based accelerator facilities as well as different Monte Carlo codes. The accelerator based experiments include dose attenuation, attenuation of the primary beam, neutron ambient dose as well as cross section measurements.

Experiment

The primary beam attenuation of several materials was tested in Cave A at GSI with 600 MeV/u carbon ions. As shown in Figure 1 the primary beam particles were counted by a 1 mm plastic scintillator before impinging on the target. Surviving carbon ions as well as the produced fragments were monitored by a dE/E telescope consisting of a 5 mm plastic scintillator and a 20 cm long BaF2 crystal scintillator.

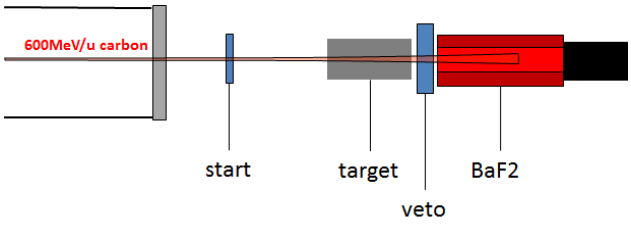

Figure 1: Schematic of the used experimental setup.

After identifying the amount of carbon ions behind the target using correlated 2D scatter plots of the telescope data and correction of the fragmentation introduced by the detectors themselves the resulting number of surviving carbon ions was calculated. Offline data analysis was performed using the ROOT data analysis framework.

Preliminary results

First preliminary results for sintered moon substitute [3] are presented exemplary in Figure 2. As expected the surviving fraction of primary beam particles is decreasing for increasing target thickness resulting in a more complex radiation field due to nuclear fragmentation. A precise knowledge of the composition of this target dependent complex radiation field is essential for space radiation risk assessment. It is important to note that the experimental error is largely dominated by the uncertainties related to the areal density of the different target thicknesses.

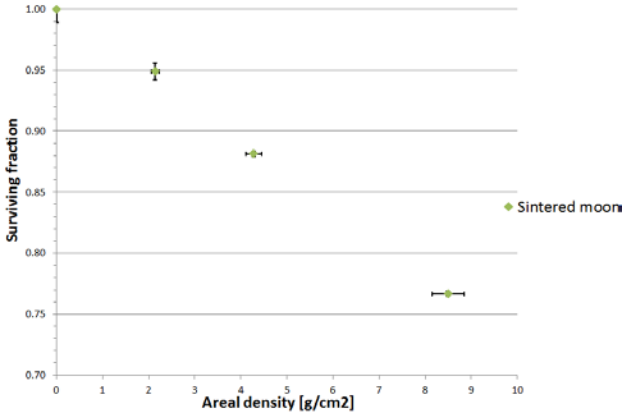

Figure 2: Preliminary results for the surviving fraction of 600MeV/u carbon ions impinging on different thicknesses of sintered moon substitute.

Status and outlook

All datasets of the different ROSSINI2 measurement campaigns are currently analyzed and compared to the widely used Monte Carlo codes PHITS and Geant4. Final results for a wide variety of different materials and beams are expected for later this year.

References

[1] M. Durante and F. A. Cucinotta, “Physical basis of radiation protection in space travel”, Rev. Mod. Phys (2011).
[2] M. Durante, “Physical and biomedical countermeasures for space radiation risk”, Z. Med. Phys (2008).
[3] Giovanni Cesaretti, et al., “Building components for an outpost on the Lunar soil by means of a novel 3D printing technology”, Acta Astronautica (2014).

* Work supported by ESA(Contr. No. 4000112525/14/NL/LF) and NASA.

Differentiation of (pre)adipocytes following irradiation*

K. Shreder[1], V. Rzeznik[1], P. Fischer-Posovszky[2], M. Wabitsch[2], C. Fournier[1]

[1] Helmholtzzentrum für Schwerionenforschung GSI, Darmstadt, [2] Universitätsklinik für Kinder- und Jugendmedizin, Sektion Pädiatrische Endokrinologie und Diabetologie, Ulm

Introduction

Rheumatoid arthritis (RA) is a chronic inflammatory disease, which affects the joints. RA patients are treated primarily with drugs, but also ionizing radiation is used. The patients are exposed either locally to low doses of photons or to Radon. Adipocytes, the dominant cell type of adipose tissue, are known to support inflammatory processes and cartilage degradation in RA by release of different cytokines and adipokines [1]. As there are no data available about the radiation response of adipocytes, we investigated in this study the effect of X-ray irradiation on the differentiation process of human (pre)adipocytes.

Materials and methods

SGBS cells were derived from subcutaneous fat of a patient with Simpson-Golabi-Behmel syndrome [2]. The cells were grown in the DMEM/F12 medium, containing 10% FCS until reaching confluence. Adipogenic differentiation was induced by addition of a defined adipogenic cocktail, including insulin and rosiglitazone. Mature adipocytes were identified by Oil Red O staining. Irradiation was performed with X-rays (1Gy/min). Gene expression was analyzed using real-time PCR.

Results and discussion

Proliferation of SGBS pre-adipocytes after X-ray irradiation

In order to assess the radiation response of pre-adipocytes, the cells were irradiated with 0.5 and 2 Gy, and the proliferation capacity was monitored over 21 days. The cell numbers of irradiated SGBS-pre-adipocytes were dose-dependently reduced (Fig. 1), which was detectable from day 12 on.

Effect of X-ray irradiation on the expression of differentiation markers

To investigate the impact of X-ray irradiation on the differentiation process of adipocytes, SGBS pre-adipocytes were irradiated with 0.5 and 2 Gy and the differentiation was initiated. Gene expression analysis of important adipogenic transcription factors PPARγ (Fig. 2) and C/EBPα (Fig. 3) revealed only slight trends towards reduced expression levels.

Our results demonstrate radiation-induced changes in the proliferation capacity of SGBS pre-adipocytes, but based on the expression of crucial adipogenic genes (PPARγ and C/EBPα) this is not accompanied by changes in differentiation.

Our data is in agreement with Nicolay et al, who showed that the expression of adipogenic genes in mesenchymal stem cells (adipocyte precursor cells) after irradiation remained unchanged [3].

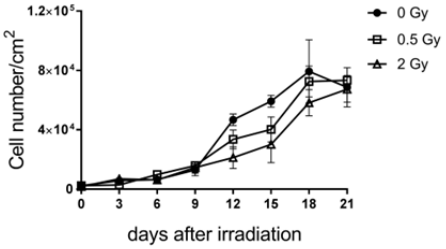

Figure 1: Proliferation of SGBS pre-adipocytes after X-ray irradiation, Mean±SEM, N=3

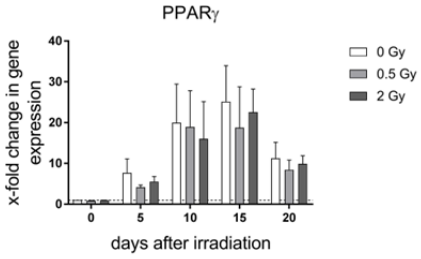

Figure 2: Gene expression of PPARγ in SGBS adipocytes following X-ray irradiation, Mean±SEM, N=3

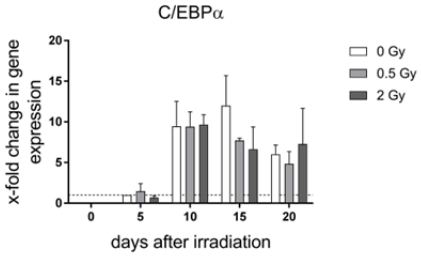

Figure 3: Gene expression of C/EBPα in SGBS-adipocytes following X-ray irradiation, Mean±SEM, N=3

References

[1] S. Vielma et al, Int. Immunopharmacol. 2013 Jun, 16(2): 224-231
[2] M. Wabitsch et al, Int. J. Obes. 2001, 25: 8-15
[3] N. Nicolay et al, Oncotarget 2014 Dec

*Work supported by BMBF (02NUK017A GREWIS)

DOI:10.15120/GR-2017-1

Low-dose irradiation reduces inflammatory reactions in endothelial cells*

Felicitas Rapp[1], Nadine Erbeldinger[1], Stephanie Hehlgans[3], Svetlana Ktitareva[1], Bianca Bertulat[2], M. Cristina Cardoso[2], Franz Rödel[3], Claudia Fournier[1]

[1]GSI, Biophysik; [2] Fachbereich Biologie, Zellbiologie und Epigenetik, TU Darmstadt; [3]Klinik für Strahlentherapie und Onkologie, Molekulare Strahlenbiologie, Goethe-Universität Frankfurt

Introduction

Patients with chronic inflammatory diseases can be treated with low doses of irradiation, either with classic X-rays or α-particles from Radon-containing water or air. Treatment leads to pain relief and anti-inflammatory effects [1, 2]. During inflammation, stimulation with cytokines (e.g. TNF-α) or irradiation, endothelial cells (EC) regulate expression of surface molecules. This fosters adhesion of peripheral blood lymphocytes (PBL), followed by transmigration through the blood vessel wall into injured tissue [3]. We have previously shown that PBL adhesion to EC is decreased after low dose exposure under laminar shear stress (blood flow) conditions, and have started to elucidate underlying mechanisms like ROS (reactive oxygen species) production and NF-κB signaling.

Methods

PBL adhesion was measured as described before [4, 5]. The production of ROS was measured in endothelial hybridoma cells (Ea.hy926) as well as primary human microvascular cells (HMVEC) via flow cytometry using an intracellular dye [1]. NF-κB translocation as an indicator for induction of gene expression was measured in Ea.hy926 and HMVEC by a high-content/high-throughput imaging routine (Operetta) 1 or 24 h after addition of TNF-α and/or photon irradiation [4, 5].

Results

Decreased PBL adhesion after low LET He-ion irradiation (76 keV/µm), comparable to α-particles, could be verified in two experiments (Fig. 1). Under laminar conditions resembling blood flow (B), this effect was more pronounced as compared to static conditions (A).

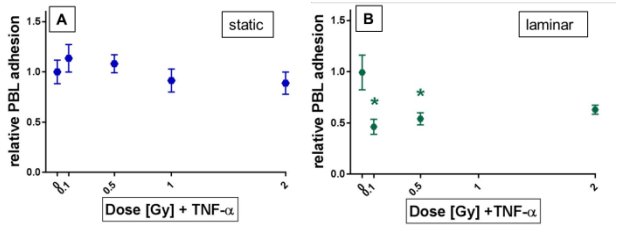

Fig. 1: Reduced adhesion of PBL to HMVEC under static (A) and laminar (B) conditions after low doses of He ions (89 keV/µm, 0.1 and 0.5 Gy, 24h). Laminar culture conditions seem to enhance the anti-inflammatory effect of low dose irradiation. Results are mean ± SEM; N=2, n=6; * p= 0.05 vs. 0Gy+TNF- α

ROS production in Ea.hy926 as wells as HMVEC follows a non-linear dose-response relationship after low doses of He-ions (Fig. 2), while the hybridoma cells show a stronger reaction than primary cells.

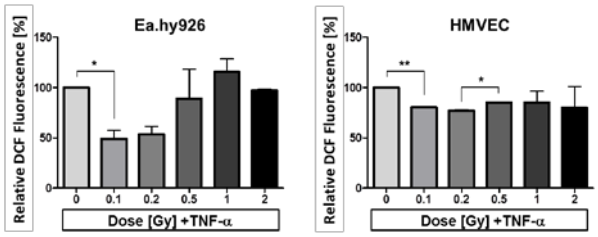

Fig. 2: Ea.hy926 or HMVEC cells were cultivated under static conditions, irradiated with He- ions (76 keV/µm) and analyzed for intracellular ROS production by flow cytometry 24 h later. ROS production is decreased at 0.1 Gy. Results are mean ± SEM; N=2, n=6; *$P < 0.05$; ** $P < 0.01$.

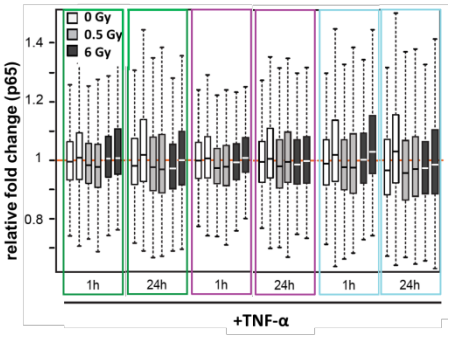

Fig. 3: Nuclear translocation of NF-κB subunit p65 after static cultivation of HMVEC, X-irradiation and TNF-α stimulation. N=1, n=3, median ± SEM.

NF-κB p65 nuclear translocation under static conditions is enhanced in the presence of TNF-α, but not further modified by low dose exposure (Fig. 3; [4]).

Discussion

We showed previously that low doses of photons reduced TNF-α- induced PBL adhesion to Ea.hy926 [1]. Here, we used low LET He-ion irradiation on primary HMVEC to mimic Radon treatment. Choosing more physiological culture conditions (Fig. 1 B) resulted in a stronger decrease of PBL adhesion to primary cells. The underlying mechanism of adhesion molecule expression is regulated by components of the antioxidative system. ROS production after He-ion exposure also showed a non-linear dose-response relationship (Fig. 2, [1]). Investigations on the respective impact of He-ion exposure, as well as on the activation of adhesion molecules, are under work.

References

[1] Large M et al., (2015) Strahlenther Onkol. 191(9):742-9.
[2] Rühle PF et al., (2017) Autoimmunity. 50(2):133-140.
[3] Schnoor et al., (2015) Mediators Inflamm. 2015:946509.
[4] Erbeldinger et al., GSI report 2015
[5] Erbeldinger et al., (2017) Front. Immunol. 8:627. (in press)

*Financed by BMBF (GREWIS 02NUK017A and 02NUK17D), DFG (GRK 1657) and HGS-HIRe
DOI:10.15120/GR-2017-1

RNF138 stimulates DNA-end resection upon heavy-ion-irradiation in human G1-phase cells

C. Barent[1,2], L. Niederreiter[1,3], L. Pack[1], A. Heselich[1], B. Jakob[1], G. Taucher-Scholz[1,2], and N. B. Averbeck[1]

[1]GSI Helmholtzzentrum für Schwerionenforschung, Darmstadt, Germany; [2]Technische Universität Darmstadt, Germany; [3]Hochschule Darmstadt University of Applied Sciences, Germany

Cells have evolved multiple DNA repair pathways to preserve genome integrity when damage arises. The most serious form of DNA damage are double-strand breaks (DSBs). Among other factors the repair pathway choice is influenced by the complexity of the break as well as the cell-cycle phase. Simple DSBs are repaired resection dependent only in the S/G2 cell-cycle phase, whereas at complex DSBs resection dependent repair occurs also in G1-phase cells [1]. It was recently shown that the ubiquitin ligase RNF138 is required for DNA-end resection in S/G2 phase in the context of RNF138-dependent Ku removal from DSBs [2]. Moreover, the ubiquitination of the resection factor CtIP by RNF138 is essential for the recruitment of CtIP to DSB sites [3]. Hence, we investigate whether RNF138 is required for resection in G1-phase cells upon induction of complex DSBs as well.

To study a possible function of RNF138 in G1 phase, it is required to be expressed in this phase. Hence, we applied the Hela.S-Fucci cell system to evaluate the RNF138-expression level in G1-phase cells in comparison to S/G2-phase cells. The Hela.S-Fucci system allows to easily distinguish and separate G1- (red) and S/G2/M-cells (green) [4] (Fig. 1 A, B, D). Protein expression studies of RNF138 showed no difference between the indicated cell cycle phases (Fig. 1 C).

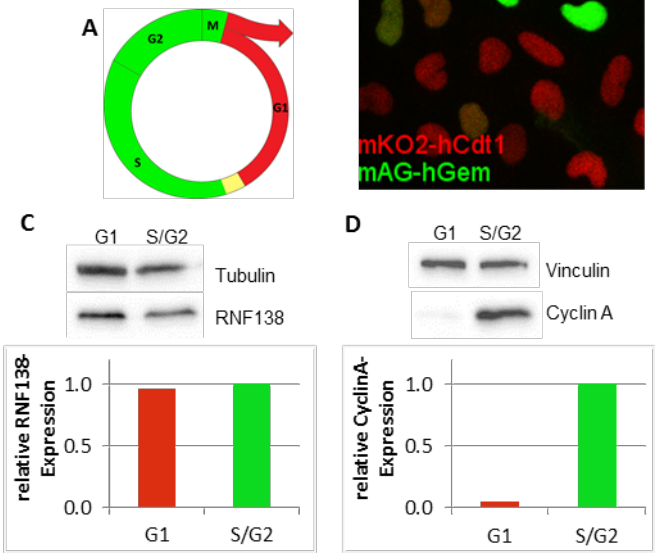

Figure 1: Hela.S-Fucci cells express RNF138 in G1- and in G2-phase cells. (A) In the Hela.S-Fucci system individual G1-phase nuclei are labelled in red and S/G2/M-phase nuclei in green. **(B)** Typical fluorescence image of HeLa.S-Fucci cells expressing mKO2-hCdt1 and mAG-hGeminin in G1 and S/G2/M-phase, respectively. **(C)** Expression of RNF138 in G1 and S/G2 HeLa.S-Fucci cells isolated via a flow cytometric sort. **(D)** The correct sorting was verified by the expression of the S/G2-marker Cyclin A. Tubulin and Vinculin served as a loading control, respectively. The quantitative evaluation was carried out with the ImageJ software. The Hela.S-Fucci cell line was kindly provided by the RIKEN BRC through Atsushi Miyawaki (RIKEN Brain Science Institute, 2-1 Hirosawa, Wako, Saitama 351-0198, Japan).

In addition, human cells depleted for RNF138 by RNAi were irradiated with carbon ions to investigate the recruitment of the resection marker RPA to DSBs. The decreased fraction of Rad51-positive cells upon irradiation (data not shown) proved the successful RNF138 knockdown. RNF138 depleted cells showed less RPA-positive cells regardless of the cell cycle phase (Fig. 2). These data suggest that RNF138 stimulates resection of complex, ion-induced DSBs in G1-phase cells. Future experiments will characterise the role of RNF138 in the repair of ion-induced DSBs in human G1-phase cells.

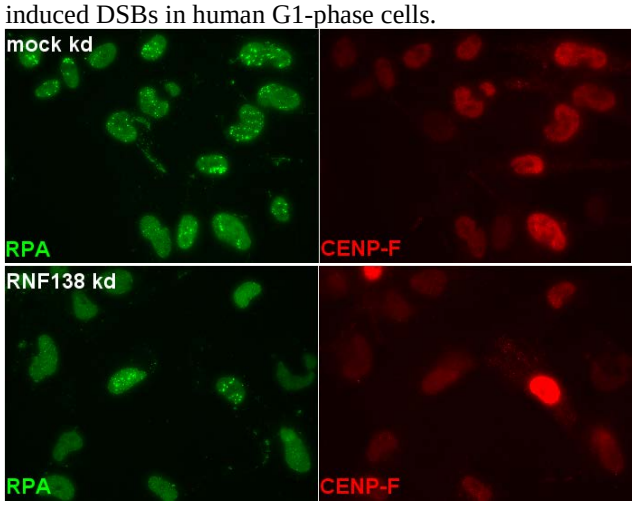

Figure 2: Depletion of RNF138 decreases the fraction of resection positive cells regardless of the cell cycle phase. Human, immortalized fibroblasts (NFFhTERT cells) depleted for RNF138 (RNF138 kd) or mock depleted (mock kd) were irradiated angular with carbon ions (6,5 MeV/u, LET: 325 keV/µm). In RNF138 depleted cells the fraction of RPA-positive cells was reduced 1 h post irradiation, regardless of the cell cycle phase. CENP-F served as a cell cycle marker (G1: CENPF-negative; S/G2: CENP-F-positive).

References

[1] Averbeck, N. B. et al. (2014). Cell Cycle **13**: 2509-2516
[2] Ismail, I. H. et al. (2015). Nat Cell Biol **17**: 1446-1457
[3] Schmidt, C. K. et al. (2015). " Nat Cell Biol **17**: 1458-1470.
[4] Sakaue-Sawano, A. et al. (2008). Cell **132**: 487-498.

* This work is supported by the DFG GRK1657 and the German federal ministry of education and research (BMBF), Grant # 02NUK037A.

DOI:10.15120/GR-2017-1

Impact of the lateral dose profiles on scanned dose distribution in particle therapy

M. Rovituso[*1,2], *C. Schuy*[1], *S. Brons*[3], *and U. Weber*[1]
[1]GSI, Darmstadt, Germany; [2]TIFPA, Trento, Italy; [3]HIT, Heidelberg, Germany

The delivery of the prescribed dose to the tumor volume is, often, realized by active techniques which consist in scanning the tumor volume slice-by-slice, with a narrow pencil beam over a matrix of single positions (raster points). The complex task to delivery an uniform dose to the tumor volume is performed by the Treatment Planning System (TPS), which needs detailed information on the beam energy, symmetry and size. The beam profile has to be parametrize with certain function in the TPS in order to be able to reproduce the core of the distirbution given by multiple Coulomb scattering and the halo given by the nuclear interaction of the beam projectile with the target nuclei. Recently a great effort is devoted to enhance the accuracy of the parametrization inside the TPS in order to better describe the contribution of the nuclear interactions in the halo region [1, 2].

This work wants to show the impact of the lateral beam shape in a scanned field. Therefore, measurements of radial dose distribution of a scattered protons and Helium beams have been performed at the Heidelberg Ion Therapy (HIT) center. The used experimental setup is explained in [2].

The data obtained for proton and ^{4}He beam at 200 MeV/u impinging on 13.96 cm H_2O have been fitted with a simple gaussian and a double Gaussian + exponential function. The result for the proton case is shown in Fig.1.

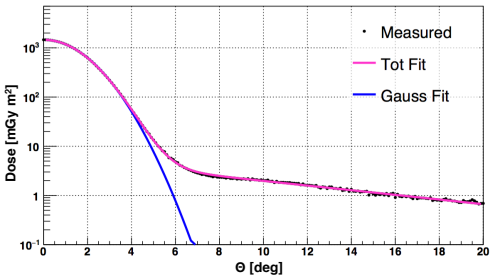

Figure 1: Fit of the radial dose distribution of 200 MeV/u proton beams impinging on 13.96 cm H_2O.

In order to quantify the effect of the parametrization on a scanned field, a 2D dose distribution was built by superimposing the beam projection distribution and shifting the beam spot in steps of 2.5 mm in x- and y-direction inside a square (target volume) size of 100x100 mm^2 and in a smaller square of 60x60 mm^2. This provides a simplified estimation for a real scanning procedure in therapy, allowing a qualitatively description of the contribution of dose transported outside the target volume due to the tail of the radial dose distribution. The results are shown in Fig.2. In order to be able to compare the Gaussian and the measured dose profile, the beam spots were superimposed with the same constant weights. It can be observed in Fig.2(a) and (c) how the effect of a single Gaussian approach affects the border of the distribution, being more pronounced for the helium dose distribution (Fig.2(a)) than for the proton one. By decreasing the target volume (Fig.2(b) and (d))the effect increases also in the plateau of the distribution, reducing significantly the dose accuracy in the target volume.

Even though the dose fall off at the border of the dose distribution for the proton beam is larger compared to ^{4}He ions, the tail contribution due to secondary fragments is higher [3], demonstrating how important is a correct parametrization of the lateral beam profile in the TPS beam models.

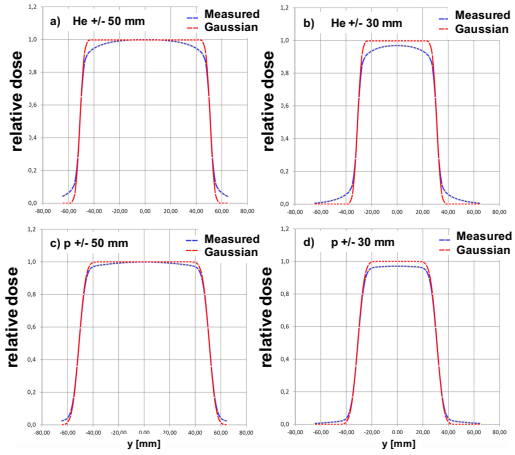

Figure 2: Dose profile through the mid plane of the scanned dose distribution for 200 MeV/u ^{4}He and proton beams.

References

[1] V.E. Bellinzona et al., "On the parametrization of lateral dose profiles in proton radiation therapy", Phys Medica, vol.31,pp.484-492, February 2015

[2] M. Rovituso et al , "Lateral scattering of 120 and 200 MeV/u ^4He ions in water", GSI Annual Report, APPA-HEALTH-36, 2016 (2013) 56

[3] M. Rovituso et al. , "Fragmentation of 120 and 200 MeV/u ^4He ions in water and PMMA targets ", Phys. Med. Biol., 62, 2017

* Work supported by HGS-HIRe

Effective cell killing following spread-out Bragg peak Carbon-ion irradiation despite efficient DNA double-strand-break rejoining

N.B. Averbeck[1], J. Topsch[2], M. Scholz[1], W. Kraft-Weyrather[1], B. Jakob[1], G. Becker[1], G. Taucher-Scholz[1,3]

[1]GSI Helmholtzzentrum für Schwerionenforschung, Darmstadt, Germany; [2]IZKS, Universitätsmedizin der Johannes-Gutenberg-Universität, Mainz, Germany, [3]TUD, Darmstadt, Germany

Radiotherapy of solid tumours aims at destructing the cancer while sparing healthy tissue. On the molecular level, DNA damage and in particular DNA double-strand breaks (DSBs) represent a crucial factor of cell killing and thus radiation effectiveness. In order to study the DSB-repair capacity and cell survival in tumour compared to healthy tissue under radiotherapy conditions with Carbon ions, we developed an irradiation setup that mimics a two-field configuration typical for patient irradiation (Fig. 1). Positions close to the beam entrance ("entrance channel", EC) represent those of healthy tissue in tumour therapy; those in the spread-out Bragg peak (SOBP) represent the tumour. Cells in the EC are exposed to a relative homogenous radiation field of high-energy ions, cells in the SOBP are exposed to a wide spectrum of Carbon ions with different individual energies and LET. Hence, DNA damage in the EC is rather simple, while damage in the SOPB ranges from simple to complex lesions.

We analysed the clonogenic cell survival and DSB repair at the EC and SOBP. Clonogenic survival is clearly lower in the SOBP compared to the EC (Fig. 2, bottom, circles). This data agrees well with the calculated survival from the local effect model (LEM) [1] (Fig. 2, bottom, line).

DSB-repair was analysed by measuring the immunofluorescence signal of the DSB marker γH2AX at different time points after irradiation by flow cytometry. Upon 2 Gy irradiation, DSBs were rejoined efficiently (Fig. 3).

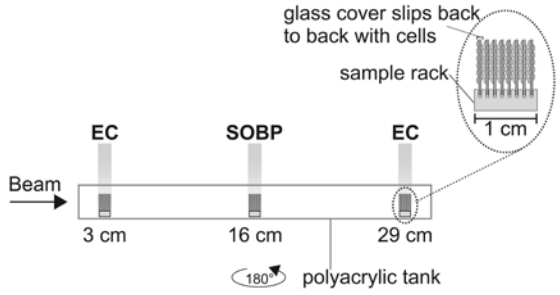

Figure 1[#]: Experimental setup for a two-field irradiation that mimics therapy-like carbon-ion irradiation. Confluent, human fibroblasts (AG1522D) were exposed at different positions from the beam entrance side within a medium filled tank at the SIS, GSI Darmstadt. To simulate a two-field configuration, the tank was irradiated with a horizontal turn of 180°. The irradiation was done with an SOBP of 2.4 cm at a water equivalent depth of 16 cm. The dose in the SOBP was 2 Gy (dose-averaged LET: 70 – 85 keV/µm), typical for a therapeutic fraction. Samples in the EC region were irradiated with a corresponding dose of 0.6 Gy (dose-averaged LET: 13 keV/ µm; see Fig. 2, top).

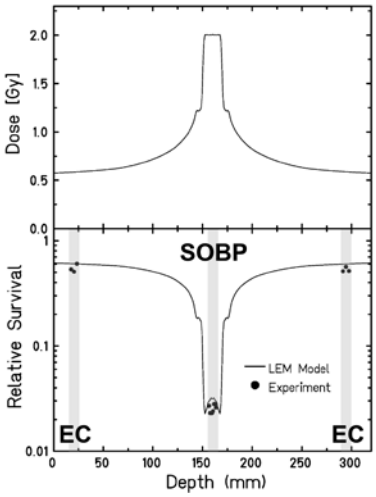

Figure 2[#]: Dose distribution and cell survival upon therapy-like irradiation as in Fig. 1. Top: Distribution of the absorbed dose. Bottom: Corresponding calculated (line; LEM) and measured (circles; n=1) cell survival. Grey boxes: position of the samples during irradiation.

The γH2AX signal declined almost to control values within 48 h in the EC and SOBP despite the increased fraction of complex lesions in the latter. Only, in the SOBP the process was slower within 24 h after irradiation. Since the lesions in the SOBP are well rejoined and yet seem to cause low survival, we assume that misrepair plays a non-negligible role in the increased cell killing in the SOBP.

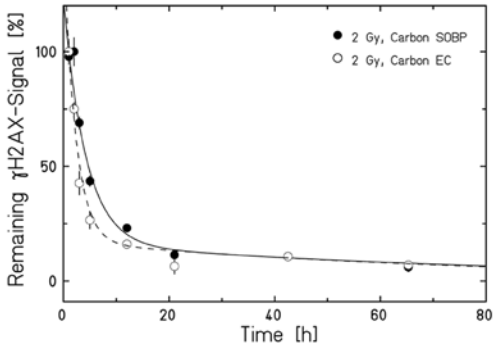

Figure 3*: Comparison of the DSB-repair capacity in human fibroblasts after 2 Gy carbon-ion irradiation in the EC or SOBP (for irradiation conditions see Fig. 1A). The global immunofluorescent γH2AX-signal was analysed by flow cytometry as described earlier [2].

References

[1] T. Elsässer *et al.*, Int J Radiat Oncol Biol Phys (2010) 78: 1177 - 1183

[2] F. Tommasino *et al.*, PLoS One (2015) 10 (6): e0129416

[3] N. Averbeck *et al.*, Front. Oncol. (2016) 6: 28

#modified version of Fig. 2 in [3]; *modified version of Fig. 3 in [3]

DOI:10.15120/GR-2017-1

Changes in cellular organization leading to the interruption of conductivity in a pig model after exposure to high doses of carbon ions

N. Erbeldinger[1,4]; P. Simoniello[1,6]; F. Rapp[1]; H. I. Lehmann[2]; P. Lugenbiel[3]; A. Eichhorn[1]; D. Thomas[3]; D. L. Packer[2]; M. Durante[5]; C. Graeff[1] and C. Fournier[1]

[1]GSI, Darmstadt, Germany; [2]Mayo Clinic/St. Marys Hospital, Rochester, MN, USA; [3]Heidelberg University Hospital, Heidelberg, Germany; [4]Darmstadt University of Technology, Darmstadt, Germany; [5]TIFPA Trento Institute for Fundamentals Physics Applications, Trento, Italy; [6]University of Naples Parthenope, Naples, Italy

Introduction

The increasing age of the population of developed countries entails higher prevalence of cardiac arrhythmias (CA). Most common CA is atrial fibrillation and ventricular tachycardia[1,2]. The first line of treatment of CA is mainly based on anti-arrhythmic and anti-coagulant medication[3]. If CA still occurs frequently, the established therapy is a minimally-invasive catheter ablation[3]. However, the efficiency of this treatment is often limited (60-75%) and comprises risks for unfavorable complications[3].

These circumstances motivated investigations on a non-invasive alternative treatment[4]. As carbon ion irradiation is well-established in cancer therapy, its benefits were exploited for this approach. First macroscopic examinations revealed scar formation in target areas in parallel to morphologically unaltered myocardium.

Based on these results, the organization of irradiated myocardium, elicited by scanned carbon ions, were investigated as cause for electrophysiological changes.

Material and Methods

The long-term effects of high dosed carbon ion irradiation on cardiac substructures were investigated in a porcine model. For this approach, targets were irradiated with single doses of 25 - 55 Gy. Follow up studies on manifold changes were performed up to six months after irradiation. For histological analyzes, tissue biopsies were obtained three and six months after irradiation during final follow-ups.

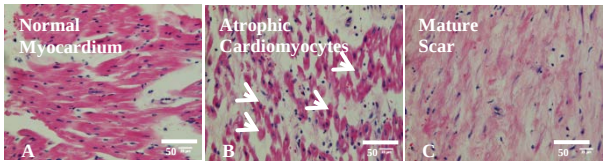

Figure 1: Different stages of cardiac fibrosis in target areas until at least 6 months after irradiation. Target areas from sham (A) and 40 Gy irradiated pigs (B, C) were stained with H&E three and six months after irradiation. Modified after[5].

Work is financed by GRK 1657 and BMBF (GREWIS, 02NUK017A)

Results

Several stages of tissue remodeling occurred in parallel in target areas. A replacement of cardiomyocytes with fibrotic tissue was observed three and six months after irradiation (Figure 1) indicating ongoing tissue remodeling. Furthermore, surviving cardiomyocytes in target areas displayed structural abnormalities. One example for those abnormalities was vacuolization (Figure 2B), which is presumably related to cell death[6]. Moreover, the distribution of the structural protein troponin the cytoplasm was inhomogeneous, indicating an altered structure of the cytoskeleton (Figure 2C, D).

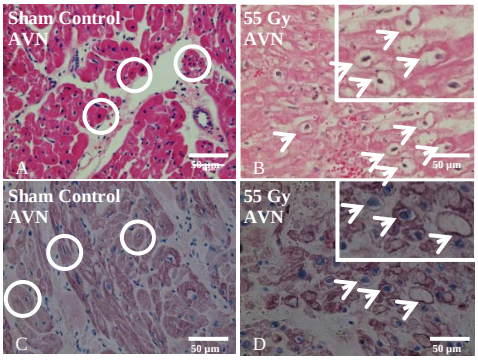

Figure 2: Vacuolization of cardiomyocytes is related to an abnormal distribution of the cytoskeleton. AVN target areas from sham (A, C) and 40 Gy irradiated pigs (B, D) were stained with H&E (A, B) and for troponin (C, D) six months after irradiation. Healthy cardiomyocytes (circles) and their vacuolization (arrows) is indicated.

Discussion

The structural abnormalities (vacuolization and distribution of troponin) of surviving cardiomyocytes point might be related to cell death during ongoing fibrosis, at late time points. In addition, cardiac fibrosis is known to cause changed electrophysiological signaling as observed in the irradiated animals. Both tissue responses (cell death and fibrosis) might underlie these changes.

References

1 Verdino J Saudi Heart Assoc. 2015 Jan; 27(1): 44–49.
2 Grant et al. Clin Geriatr Med. 2012 November ; 28(4): 539–553.
3 Cappato, Circ Arrhythm Electrophysiol. 2010 Feb;3(1):32-8.
4 Lehmann et al, Sci Rep. 2016 Dec 20;6:38895.
5 Erbeldinger, doctoral dissertation, submitted 2017
6 Vigliano et al,, J Am Coll Cardiol. 2011 Apr 5;57(14):1523-31.

TRAX-CHEM*

D. Boscolo†[1], *E. Scifoni*[2], *M. Krämer*[1], *and M. Durante*[2]
[1]GSI, Darmstadt, Germany; [2]TIFPA, Trento Italy

Although it is well known that the indirect effect of radiation plays a very important role on the radiation effect on biological systems and many dosimetrical technique are based on the detection of chemical reactions with radiation induced free radicals, still little is known on water radiolysis and on radicals diffusion and reaction along a particle track. For this reasons in the last two years the particle track structure code TRAX [1] has been extended to the pre-chemical and chemical stage of radiation damage [3][4]. It is now possible to use this extension of the code in order to simulate the time-dependent yields of the most important products of water radiolysis e^-_{aq}, $\cdot OH$, $H^\cdot$, H_3O^+, H_2, OH^- and H_2O_2 for different ion radiation and different energies. In Figure 1 the computed time dependent G-values for different radical species generated by a 750keV electron are compared with experimental data.

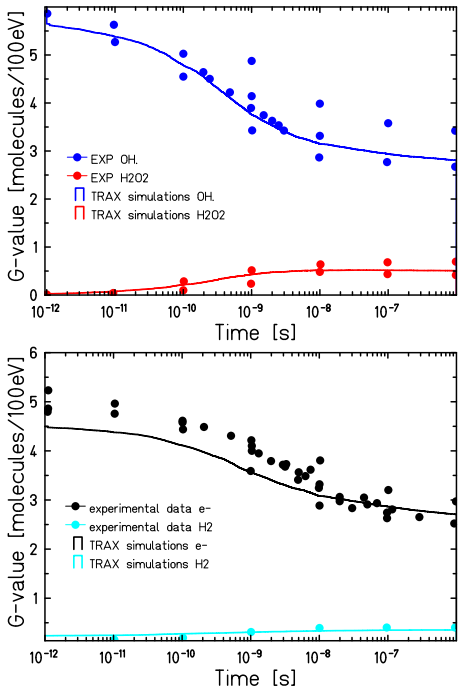

Figure 1: Time-dependent radiolytic yields for 750keV electron in a water cube of 5 μm side for the species $\cdot OH$ and H_2O_2(top panel) and e^-_{aq} and H_2 (bottom panel). Experimental data from [2].

With the increase of the LET the particle track becomes more dense increasing the probability or radical recombination. This will lead to a decrease of the G-values of radical species generated immediately after the water dissociation, such as $\cdot OH$ and e^-_{aq} and to an increase of the radical generated by the interaction of the former ones, such as H_2O_2 and H_2. A comparison of the LET dependent G-values at the end of the chemical stage with experimental data is shown in Figure 2 for different radical species. The OH radical yield depending on both time and LET seems to be in very good agreement with the experimental data while for the other radicals some refinements are still required especially to predict their yield for high LET radiation.

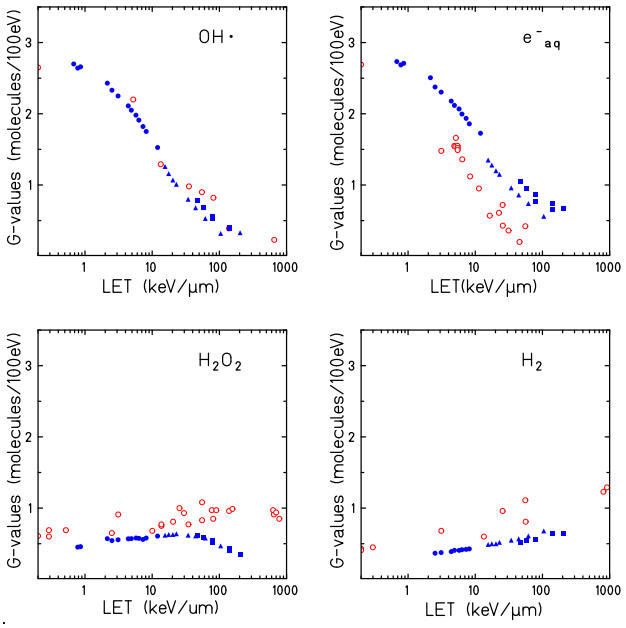

Figure 2: LET dependence of G values in pure water for the species $\cdot OH$(top left) , e^-_{aq} (top right), H_2O_2(bottom left) H_2 (bottom right). Solid blue symbols :TRAX simulations (circle 1H, triangle 4He, square 12C). Open red circles: collection of experimental data from [2]

References

[1] C.Wälzlein et al., Phys. Med. Biol. ,59:1441-1458(2014).
[2] M.S.Kreipl et al., Radiat. Environ. Biophys. ,48:11-20(2009).
[3] D.Boscolo, et al. "Chemical stage implementation in TRAX", GSI Scientific Report 2015 (2016)
[4] M.Bolsa, et al. Chapter in book: "Nanoscale Insights into Ion-Beam Cancer Therapy", pp.379-434, (2017)

*The research leading to these results has received funding from the European Union Seventh Framework Programme [PEOPLE 2013 ITN-ARGENT project] under grant agreement n [608163].
† d.boscolo@gsi.de

DOI:10.15120/GR-2017-1

Advanced IMPT algorithm for multiple targets of late stage lung cancer

K. Anderle[1], *J. Stroom*[2], *S. Viera*[2], *N. Pimentel*[2], *C. Greco*[2], *M. Durante*[3] and *C. Graeff*[1]
[1]GSI, Darmstadt, Germany; [2]Champalimaud Centre for the Unknown, Lisbon, Portugal; [3]TIFPA, INFN, University of Trento, Povo (TN), Italy;

Introduction

Patients with late stage lung cancer have extremely poor prognosis, with median survival rate less than a year, therefore new treatments are warranted. Recent studies have shown promising results with stereotactic body radiation treatment (SBRT) for such patient patients [1], however patients still exhibit several radiation-induced side effects.

With better physical properties for radiotherapy, intensity modulated particle therapy (IMPT) could better spare normal tissue. However, creating a treatment plan for moving tumours in complex geometries is challenging, due to range changes and interplay effects.

To address these challenges, an algorithm was developed to create IMPT treatment plans for late stage lung cancer patients. To asses the developed algorithm, the generated plans were compared to SBRT ones, which were used in an actual treatment.

Materials and Methods

Our algorithm was implemented in the GSI's treatment planning software, TRiP98 [2]. Firstly, modifications were made to the raster point setup, where previously only one target was supported. Raster point setup was expanded in a way that every field is designated to a specific target. Raster points for each field are created only around the designated target. Afterwards optimization takes into account contributions from all fields. The opti mization function was adapted so that strict stereotactic treatment planning objective could be respected.

By optimizing over all motion states, range changes are already included [3]. Rescanning was used to address interplay changes. After successful optimization, a time-resolved (4D) dose was calculated, to quantify motion effect on the treatment. Furthermore, dose was calculated on 4 different motion variations to estimate plan robustness.

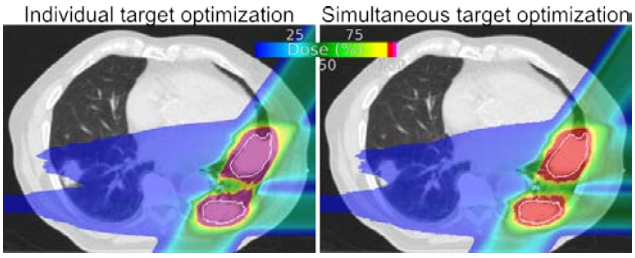

Figure 1 - Comparision between individual and simultaneous target optimization.

To test the algorithm, IMPT treatment plans for 8 patients with 24 lesions in total were generated. Patients were actually treated with SBRT at Champalimaud Center for the Unknown, Lisbon, Portugal. Intended dose regimen for SBRT was 24 Gy in 1 fraction, but lower fractionated doses had to be delivered in 3 cases due to OAR constraints. Besides adopting the fractionation regimes for IMPT, additional dose escalation of 1x24Gy was explored for these 3 cases.

Results

A comparison between IMPT and SBRT treatment plans for two patients is shown on Figure 2. Patient 2 has no critical OARs in close vicinity to the target and both modalities deliver the same dose to 5 targets. IMPT for Patient 5 has poorer target coverage for two targets close to the heart. Both patients receive less integral dose in the whole body with IMPT.

Overall, there was no significant difference in target coverage between SBRT and IMPT. However, the IMPT on averaged deposited 44% and 70% less dose to OARs for maximum point dose and dose to critical volume, respectively.

A dose escalation was possible for one patient with large overall target volume, where an IMPT plan of single fraction could be created and SBRT was limited due to high heart dose. This shows the potential of IMPT for late stage lunge cancer patient.

Conclusions

An advanced optimization algorithm was developed and used to achieve superior IMPT treatment plans for late stage lung cancer patients. Furthermore, IMPT could be used in a single fraction regime for some patients, where SBRT was limited.

References

[1] Iyengar P, et al: Phase II Trial of Stereotactic Body Radiation Therapy Combined With Erlotinib for Patients With Limited but Progressive Metastatic Non–Small-Cell Lung Cancer. Journal of Clinical Oncology 32, 2014
[2] Krämer M, et al: Treatment planning for heavy-ion radiotherapy: calculation and optimization of biologically effective dose. Physics in Medicine and Biology 45, 2000
[3] Graeff C, et al: Motion mitigation in intensity modulated particle therapy by internal target volumes covering range changes. Med. Phys 39, 2012

DOI:10.15120/GR-2017-1

Ionizing radiation alters signalling pathways affecting the maintenance and endodermal differentiation of embryonic stem cells.*

S. Luft[1], O. Arrizabalaga[1], Ireen Kulish[1,2], E. Nasonova[1,3], M. Durante[4], S. Ritter[1], I. Schroeder[1,#]

[1]GSI, Darmstadt, Germany; [2]Technical University Darmstadt, Darmstadt, Germany; [3]Laboratory of Radiation Biology, Joint Institute for Nuclear Research, Dubna, Russia; [4]Trento Institute for Fundamentals Physics Applications (TIFPA), Trento, Italy.

We investigated the impact of ionizing radiation (IR) on the properties of human embryonic stem cells (hESCs) and their capability to differentiate into definitive endoderm (DE) that will eventually give rise to organs such as the lung, pancreas and liver. The usage of hESCs allowed us to mimic early development *in vitro* (Figure 1). Thus, the study addressed a very radiation-sensitive period of the embryogenesis as the ability of hESCs to preserve genomic integrity and to form any tissue of the body is crucial for proper embryonic development. Any disturbance of this process may lead to functional defects, malformations, cancer or premature death. IR is a known disturbing factor in early development but the underlying mechanisms have yet to be elucidated in detail.

In the above mentioned study we identified for the first time the mechanism that led to altered stem cell properties and impaired capacity to differentiate into DE of irradiated hESCs. Exposing hESCs to X-ray irradiation (1Gy and 3 Gy, respectively) led to immediate responses such as a cell cycle arrest in G2/M phase, elevated apoptosis and increased chromosomal aberrations. However, these effects were transient and mostly overcome within 24h.

In contrast, stem cell signalling analyses revealed changes in the TGF beta-, Wnt-, and Hedgehog pathways that persisted up to four days in case of irradiation with 3Gy. Remarkable was the down-regulation of activin receptors. They not only regulate the maintenance of pluripotency, the ability to form all tissues of the body, but also the differentiation of hESCs into DE. Accordingly, surviving hESCs, which were differentiated 4 days post-irradiation, showed a lower efficiency to form DE than their mock-irradiated counterparts. This was conclusively demonstrated by a reduced expression of the key regulator of DE formation, SOX17 and the microRNA miR-375.

However, the study also revealed that hESCs responded differently to IR depending on the culture conditions chosen for maintenance (Figure 2): enzymatically passaged cells, representing the most commonly used hESCs, were less sensitive than mechanically passaged ones and showed fewer apoptotic events, fewer changes in stem cell signalling but also higher levels of chromosomal aberrations.

From our results we conclude that the enzymatically passaged cells are more inhomogeneous hampering the identification of an IR impact. Thus, careful choice of appropriate culture conditions and vigorous monitoring of the stem cell quality are mandatory for the use in radiation biology and the assessment of a radiation risk during early development.

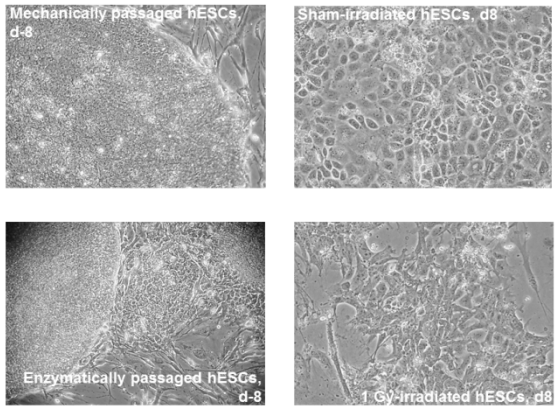

Figure 2: Morphology of cells before (d-8) and after (d8) differentiation.

The study has demonstrated that exposure to IR influences the properties of hESCs even when the immediate radiation effects are overcome. This warrants consideration in the risk assessment of radiation effects during the earliest steps of human development. For further details see Luft et al. [1].

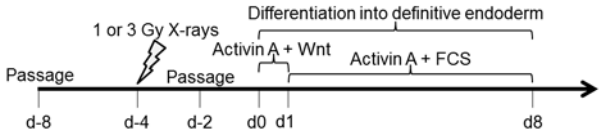

Figure 1: Differentiation and irradiation scheme

References

[1] S. Luft et al., "Ionizing Radiation Alters Human Embryonic Stem Cell Properties and Differentiation Capacity by Diminishing the Expression of Activin Receptors, Stem Cells and Development 26 (2017) 341.

* Work supported by BMBF (02NUK025A).
#i.schroeder@gsi.de

DOI:10.15120/GR-2017-1

Impact of ionizing radiation on cardiac differentiation – an update*

S. Nitsch[‡,1], *F. Braun*[1/2], *J. Kunz*[1], *S. Ritter*[1], *M. Scholz*[1], *I. Schroeder*[#,1]
[1]GSI, Darmstadt, Germany, [2]Hochschule Darmstadt, Germany

Currently embryo- and cardiotoxicity of drugs or medical treatments, like ionizing radiation, are mostly investigated in animal models. However, due to species-specific differences, data obtained from these studies are difficult to extrapolate to the human organism. Therefore, human embryonic stem cells (hESC) are one of the most important models to study embryo- and cardiotoxic effects during human development.

Previous studies of our lab used the wildtype hESC line WA09 (H9) which was differentiated into cardiomyocytes by using two different protocols [1, 2]. In 2014, Wrighton et al. established a genetically modified H9-cell line called H9-cTnT-GFP [3] which we now established in our laboratory. In these cells, GFP is under the control of the cardiac specific troponin T (TNNT2) promoter leading to green fluorescence when TNNT2 is expressed. Thereby, cardiac cells can easily be distinguished from non-cardiac cells that develop during the differentiation process to support the cardiac differentiation.

First experiments confirmed that H9-cTnT-GFP cells can be successfully differentiated into beating cardiomyocytes and express typical cardiac markers during differentiation (Figure 1). Compared to wildtype H9-cells their marker gene expression is higher.

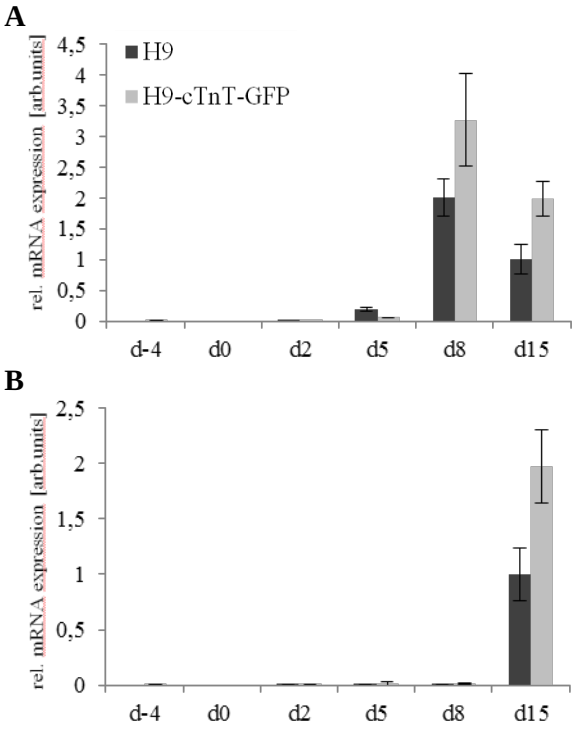

Figure 1: Relative mRNA expression of cardiac marker genes cTnT (A) and MLC2v (B) during differentiation. d=day, d0=initiation of differentiation.

Wildtype and H9-cTnT-GFP derived cardiac clusters respond to the beta-adrenoreceptor agonist isoproterenol visualized by an increased beating rate (Figure 2), thereby confirming the presence and functionality of these receptors and their ability to respond to exogenous factors.

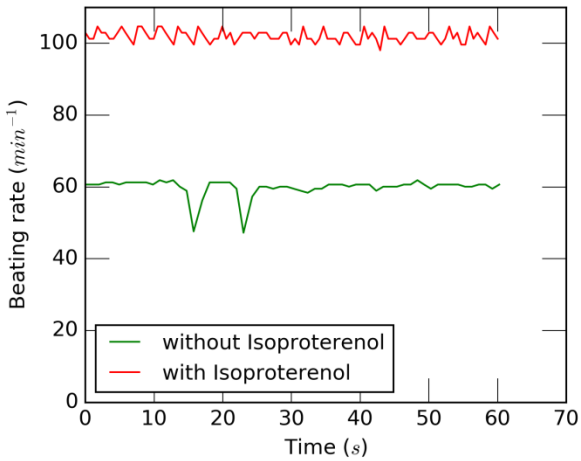

Figure 2: Beating rate of one cardiac cluster derived from H9-cTnT-GFP before (lower line) and after (upper line) stimulation with 1 µM isoproterenol.

Based on their fluorescence signal, cardiac cells derived from H9-cTnT-GFP can be separated from the supporting, non-fluorescent cells by Fluorescence Activated Cell Sorting (FACS). This allows for the specific analysis of these cell types regarding their marker gene expressions.

In conclusion, H9-cTnT-GFP cells behave similar to the wildtype cells and are therefore suitable to investigate effects of ionizing radiation on the differentiation of hESC.

References

[1] Kadari et al., Robust Generation of Cardiomyocytes from Human iPS Cells Requires Precise Modulation of BMP and WNT Signaling. Stem Cell Rev and Rep 2015, 11:560

[2] Lian et al., Directed cardiomyocyte differentiation from human pluripotent stem cells by modulating Wnt/β-catenin signaling under fully defined conditions. Nature Protocols 2013, 8:162

[3] Wrighton et al., Signals from the surface modulate differentiation of human pluripotent stem cells through glycosaminoglycans and integrins. PNAS 2014, 51:18126

* Work supported by BMBF (02NUK025A).
‡ S. Nitsch is supported by HGS-HIRe.
#i.schroeder@gsi.de

Nonlinear robust optimization methods for 4D treatment planning in carbon ion therapy*

M. Wolf[1,2], *K. Anderle*[1], *and C. Graeff*[1]
[1]GSI, Darmstadt, Germany; [2]TUD, Darmstadt, Germany

Introduction

We introduced robust optimization into non-linear biological optimization of GSI's TRiP4D to avoid internal IMPT dose inhomogeneities. Here we present a conformal robust 4D optimization delivering a homogeneous dose to each motion phase resulting in a plan library [1]. The delivery of this set of plans has to be synchronized to the motion.

Materials and methods

The implemented worst case scenario method currently considers 9 different scenarios in the optimization process: nominal scenario, 2 range error scenarios (shifting water-equivalent path length (WEPL) by $\pm 3.5\,\%$) and 6 positioning error scenarios (shifting the patient's iso-center by ± 5 mm target in S-I, A-P and L-R direction) [2]. In every iteration step LEM-based RBE-weighted doses are calculated for all scenarios from the current set of beam fluences respecting fragment spectra and LET. Within the conformal 4D optimization approach, robust IMPT on the CTV is compared to conventional IMPT on the PTV using 5 mm isotropic margins regarding 4D dose distributions for different uncertainty scenarios. Each phase of the 4DCT is optimized individually.

Results

Using robust IMPT in a patient case with a lung tumor in close proximity to the heart, a motion amplitude larger than 2 cm and a target dose of 9.4 GyE, an increased target dose of 9.6 GyE due to the steeper falloff and smaller spread in the robust DVHs was enabled. Thus the target coverage (V95) could be increased from $87.6 \pm 10.6\,\%$ to $98.0 \pm 2.7\,\%$ averaged over all scenarios by slightly increasing mean heart dose from 0.7 ± 0.1 GyE to 0.9 ± 0.1 GyE compared to conventional IMPT (see fig. 1). The dose spread of the DVH bands could be reduced from $6.3\,\%$ to $4.5\,\%$ on the V50 value using robust IMPT.

Conclusion

An initial patient simulation shows the feasibility and the importance for robust (4D) optimization methods for moving targets in carbon ion therapy. A further extension of the algorithm to a full 4D robust optimization where all phases of the 4DCT are optimized simultaneously using deformable image registration in every iteration step will follow, completed by an expanded patient study comparing different robust 4D optimization methods.

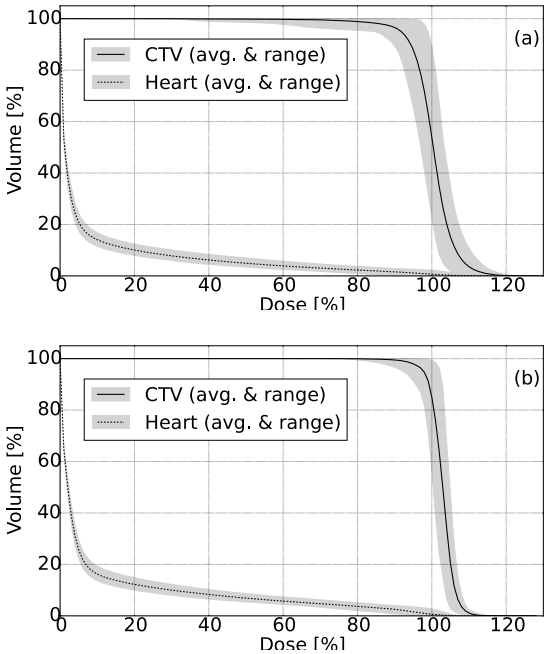

Figure 1: Dose volume histogram (DVH) for the 4D dose distribution of several error scenarios comparing for (a) conventional IMPT and (b) robust IMPT used in conformal 4D optimization. The gray bands show the uncertainties due to the error scenarios. The black lines give the DVH values averaged over all scenarios.

References

[1] C. Graeff, "Motion mitigation in scanned ion beam therapy through 4D-optimization", Phys. Med. (2014) 30, p.570-577

[2] W. Liu et al., "Robust optimization of intensity modulated proton therapy", Med. Phys. (2012) 39 (2), p.1079-1091

* Work supported by HGS-HIRe.
[1]mo.wolf@gsi.de

DOI:10.15120/GR-2017-1

BRCA1's function at complex heavy-ion induced DNA double strand breaks may include regulation of resection

T. Syzonenko[1,2], B. Jakob[1], G. Becker[1], G. Taucher-Scholz[1,2] N. B. Averbeck[1]

[1]GSI Helmholtzzentrum für Schwerionenforschung, Darmstadt, Germany; [2]TUD, Darmstadt, Germany

We observed repair relevant resection of heavy-ion induced DNA double-strand breaks (DSBs) in G1-phase cells [1]. Studying the regulation of this resection, we found earlier that BRCA1, required for break resection in G2-phase [2], is recruited to heavy-ion induced DSBs in G1-phase cells [3].

In order to study BRCA1's possible function in the resection of heavy-ion induced DSBs in G1-phase cells, we on the one hand depleted cells for BRCA1 by RNAi (Fig. 1A) and on the other hand increased the BRCA1 level by depletion of HUWE1, a negative regulator of BRCA1 [4] (Fig. 1B).

Neither increase nor decrease of the BRCA1 level had an effect on the fraction of resection positive cells upon heavy ion irradiation (Fig. 2A and B).

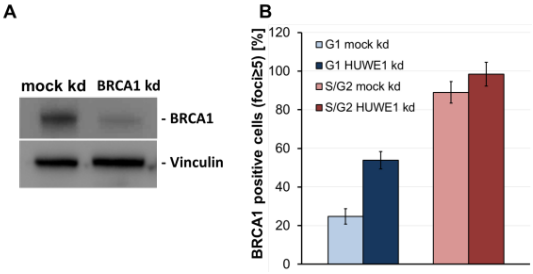

Figure 1: Decrease and increase of the BRCA1-protein level by BRCA1 knockdown (BRCA1 kd) and HUWE1 knockdown (HUWE1 kd) in U2OS cells, respectively. (A) Western analysis to proof the successful decrease of the BRCA1-protein level by RNAi. Mock depleted cells (mock kd) were treated as BRCA1 kd cells but without siRNA. **(B)** Increase of the BRCA1-protein level by RNAi driven HUWE1 depletion in G1 cells. U2OS cells were mock depleted or depleted for HUWE1 and irradiated with oxygen ions (LET 610 keV/µm, 6.5 MeV/nucleon, 5 x 10^6 p/cm^2). 1 h post-irradiated samples were fixed and stained against BRCA1 and the cell cycle marker CENP-F. BRCA1 positive cells (foci number ≥ 5) in HUWE1 depleted cells were quantified in G1 (CENP-F negative cells) or in S/G2 (CENP-F positive cells). More than 100 cells were counted in each sample. The number of BRCA1 positive cells in non-irradiated cells was subtracted. Error bar: binomial error.

Yet, determining the number of RPA foci upon irradiation of BRCA1 depleted cells revealed a resection defect in S/G2- and G1-phase (Fig. 3). Taken together, these data suggest that although BRCA1 is not a critical factor of resection of complex ion induced DSBs it is involved in regulation of their resection not only in S/G2-phase cells but also in G1-phase cells.

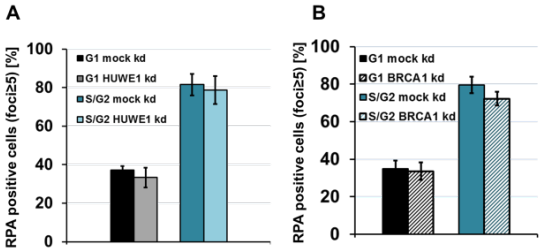

Figure 2: Fraction of resection positive cells is not influenced by modifying the BRCA1 protein level. U2OS cells were mock depleted (mock kd), depleted for HUWE1 (HUWE1 kd) **(A),** or depleted for BRCA1 (BRCA1 kd) **(B)** by RNAi and irradiated with oxygen ions (LET 610 keV/µm, 6.5 MeV/u, fluence 5 x 10^6 p/cm^2). 1 h post irradiation, the samples were fixed and stained against RPA (resection marker) and CENP-F (cell cycle marker). RPA positive cells (foci ≥ 5) were quantified in G1 (CENP-F negative cells) or in S/G2 phase (CENP-F positive cells). Graph shows mean number of RPA positive cells; n=1, error bars: binomial error.

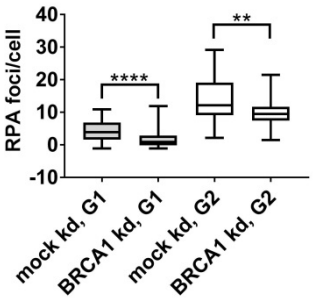

Figure 3: BRCA1 depletion decreases the RPA foci number in S/G2 and G1 cells. U2OS cells were mock depleted (mock kd) or depleted for BRCA1 (BRCA1 kd) by RNAi and irradiated with carbon ions (LET 325 keV/µm, 4.05 MeV/u, 5 x 10^6 p/cm^2). 1 h post irradiation, the samples were fixed and stained against RPA (resection marker) and CENP-F (cell cycle marker). RPA foci per nucleus were counted in at least 50 cells per sample. n=1, whiskers: minimum and maximum. Mann-Whitney test: (****) indicates P<0.0001, (**) indicates P<0.01. The average number of foci measured in non-irradiated cells was subtracted.

References

[1] N. Averbeck *et al.*, Cell Cycle (2014) 13(16): p. 2509-16.
[2] C. Escribano-Diaz *et al*., Molecular Cell (2013) 49, 1-12.
[3] T. Syzonenko *et al.*, GSI, Scientific Report 2015.
[4] Wang *et al.*, BBCR (2014) 444, 549-554.

* This work is part of the Helmholtz Graduate School for Hadron and Ion Research "HGS-HIRe for FAIR" and supported by Graduate College 1657 "Molecular and cellular responses to ionizing radiation".

Comparison of X-ray and ion irradiation dependent protein recruitment to DNA lesions using online microscopy

E. Janiel[1], *G. Becker*[1], *G. Taucher-Scholz*[1, 2], *B. Jakob*[1]
[1]GSI, Darmstadt, Germany; [2]Technical Universität Darmstadt, Germany;

Introduction

The repair of DNA lesions, especially double strand breaks (DSBs), is an essential process for maintaining genome integrity. It is tightly controlled by a complex network of DNA repair factors. Beamline microscopy of living cells with fluorescently tagged DNA repair factors revealed LET dependent recruitment kinetics for the factor NBS1, but almost no LET dependency for 53BP1 recruitment[1,2]. In the following, these findings are compared to X-ray dependent protein recruitment measurements through temporal resolved analysis of NBS1 and 53BP1 accumulation at DNA DSBs.

Materials and Methods

Living U2OS cells expressing fluorescently tagged DNA repair factors, NBS1-GFP2 or 53BP1-GFP (all kindly provided by Dr. Claudia Lukas, Danish Cancer Society, Copenhagen, Denmark), were irradiated with 0.92Gy X-rays inside a stage incubation system on the microscope. Images were captured before and immediately after irradiation, every ten seconds. The relative intensity of irradiation induced foci (IRIF) was measured above the background (average per individual nucleus) and plotted as a function of time.

Results

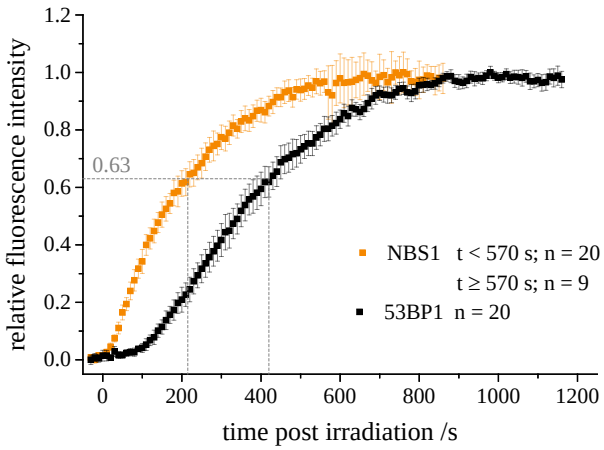

Figure 1 – Kinetics of NBS1 and 53BP1 accumulation after X-rays . X-ray irradiation at ~ 1 Gy revealed faster recruitment of NBS1 to DSBs and shorter delay than that of 53BP1 (mean intensities ± 95% confidence interval).

The live-cell recruitment measurements at X-ray induced DSBs revealed an assembly of 53BP1 in IRIFs that lags behind NBS1 accumulation (Figure 1). Average recruitment of 53BP1 exhibits a lag phase of approximately two minutes whereas average NBS1 accumulation already starts within the first 30 seconds. As shown by Tobias et al. 2013, fast protein accumulation after irradiation can approximately be described by a mono-exponential saturation curve yielding a single time constant, representing the time when 63% of the final foci intensity is reached. For NBS1 recruitment this time constant was ~220s whereas for 53BP1 a similar level was reached after ~440s due to the lag phase (dotted lines, Figure1). As compared in Tab. 1, the NBS1 mono-exponential time constants for X-ray and carbon ions are similar whereas the time constant for NBS1 recruitment at higher LET induced damage was much shorter. Concerning 53BP1, a direct relation between damage density and time constant was not observed.

Table 1 – X-ray and ion irradiation dependent recruitment times of NBS1 and 53BP1 to DNA DSBs.

	X-rays	Carbon	High LET
NBS1	220±25 s	235±25 s [(1)]	80±10 s [(1), A]
53BP1	420±35 s	640±80 s [(1)]	580±80 s [(1), B]

[(1)]) Tobias F. et al. 2013
[A] V ions, LET = 2460 keV/µm
[B] Au ions, LET = 13000 keV/µm

Conclusions

The accumulation of the DNA DSB repair factors NBS1 and 53BP1 could be observed after X-ray irradiation in real-time. The time constant of NBS1 recruitment was lower than that of 53BP1 for all compared radiation qualities. This is in agreement with the findings that NBS1 acts upstream of 53BP1[3]. NBS1 recruitment kinetics at moderate LET and X-ray induced DNA damage sites were fairly similar supporting a model of predominantly binding to the surroundings of the actual DSBs at low local DSB numbers [1]. Concerning 53BP1, the recruitment showed a pronounced delay in the order of 2 min and was rather independent of the LET. The apparently slightly faster recruitment after X-rays might be due to a more transient nature of recruitment. The different LET dependent behaviour indicates that NBS1 recruitment is not the rate limiting step for a subsequent 53BP1 accumulation.

[1] F. Tobias et al., *PLoS One* **2013**, *8*
[2] V. Hable. et al., *PLoS One* **2012**, 7
[3] S. Panier and S. J. Boulton, *Nat Rev Mol Cell Biol* **2014**, *15*, 7-18

* This work is supported by the German federal ministry of education and research (BMBF), Grant#: 02NUK037A.

DOI:10.15120/GR-2017-1

High energy proton imaging for medical applications at FAIR

M. Schanz[*1], *T. Berger*[3], *M. Krämer*[1], *N. Peters*[2], *B. Przybyla*[3], *and D. Varentsov*[1]
[1]GSI, Darmstadt, Germany; [2]Universität Halle-Wittenberg, Halle, Germany; [3]DLR, Cologne, Germany

Flash Proton Radiography with high energy protons in the GeV-range is a diagnostics technique developed in the 1990s at the Los Alamos National Laboratory (LANL) for investigations on high energy density states of matter [1]. Recent experiments have shown that it is also very sensitive in the low-density-regime making this method an ideal tool for biomedical applications such as the imaging of patients during heavy ion radiotherapy [2]. The fast data acquisition will enable live tracking of the patient which is a key feature for the treatment of moving tumors.

Experiments at LANL

In order to demonstrate and quantify the performance of proton radiography for biomedical applications, several targets were manufactured at GSI in 2016 and irradiated with 800 MeV protons at the pRad facility of the LANL. Fig. 1 shows the setup that has been used for most of the measurements. Although an unknown amount of scattering and energy straggling due to three windows, a tungsten diffuser and the air gap of 1 m where the target was placed occured, a spatial resolution of 65.3 μm was achieved. The evaluation of the data is not yet completed, but a density resolution of 1 % or less is to be expected.

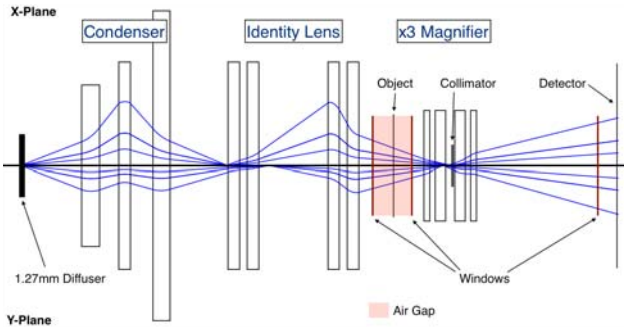

Figure 1: Ion optical scheme of the pRad facility at the LANL.

For further investigations a PMMA head phantom with different insets made of tissue equivalent plastics (see Fig. 2) was irradiated. The corresponding dose for a single projection was measured with thermoluminescence dosimeters situated in a separate target on top of the phantom (see upper part of radiograph in Fig. 2). Although the measured dose is comparably high ($D_{avg} = 52$ mGy per projection / $1.92 \cdot 10^{10}$ protons), the low noise in the acquired images indicates that a reduction of the proton dose by a factor of 100 will not affect the accuracy of the density resolution, thus permitting the operation in a clinically feasible dose range.

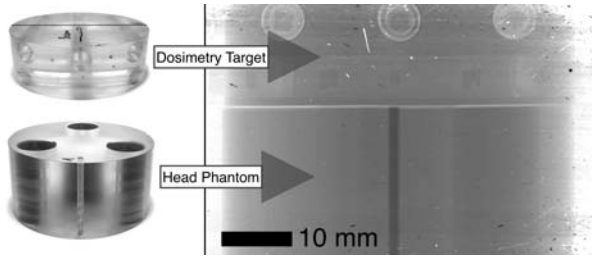

Figure 2: Head phantom and dosimetry target (left) and proton radiography (right). The insets from tissue equivalent plastic are designed to imitate soft tissue with small deviations in density from 0.36 % up to 7.56 %.

Biophysics at FAIR

During the 2018 beam time further experiments with low density static targets are planned at the HHT cave where the new PRIOR-II facility will be commissioned.

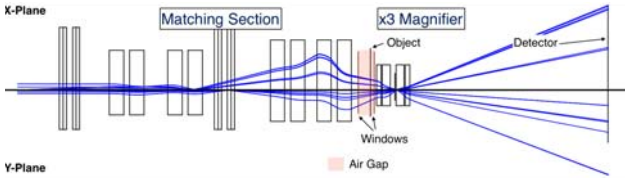

Figure 3: Ion optical scheme of the PRIOR-II facility at FAIR.

Following these investigations PRIOR-II will be transferred to the FAIR site and installed as a permanently available diagnostic system at the HEDgeHOB beam line [3]. Continuing the collaboration with the plasma physics department in the APPA cave, this facility will also be available for biophysics experiments. The new facility offers a 2.1 m gap for the installation of various experiments allowing also the examination of larger body phantoms (see Fig. 3).

References

[1] C.L. Morris et. al., “Charged particle radiography”, Rep. Prog. Phys. **4**, 2013.

[2] M. Prall et. al., “High-energy proton imaging for medical applications”, Scientific Reports **6**, 2016.

[3] M. Schanz, “High Energy Proton Microscopy at FAIR”, Master thesis, TU Darmstadt, 2016

* m.schanz@gsi.de

Inspection of counting loss and pile up effect on fluorescence lifetime recording of radiation-induced chromatin decompaction*

E. Abdollahi[1], *L. Pack*[1], *G. Taucher-Scholz*[1, 2], *B. Jakob*[1]
[1]GSI, Darmstadt, Germany; [2]Technical Universität Darmstadt, Germany;

Introduction

Recently, we provided evidence that densely ionizing radiation induces chromatin decondensation, which most probably originates as a biological consequence of DNA double strand break (DSBs) formation [1]. However, the lack of a sensitive method of detection of chromatin compaction by intensity based measurements introduced a need for the establishment of a new approach to obtain a more reliable readout. Employing fluorescence lifetime imaging microscopy (FLIM), we recently showed that chromatin compaction probes based on single organic dyes can be used to demonstrate a local radiation-induced chromatin relaxation at sites of ion traversals [2]. However, we experienced an unexpected lifetime dependency on the fluorescence and laser intensity at moderate average detector count rates. At high count rates, counting loss and pile-up effect due to detection deadtime have been reported to impair results of TCSPC FLIM [3] readout. Thus, we analyzed how these effects impact on photon numbers and lifetime distribution in our spatially inhomogeneous emitting samples under the applied conditions. In addition, we investigated in how far the detected radiation induced chromatin decompaction was impaired by the applied deadtime correction.

Material and Methods

TCSPC FLIM measurements of formaldehyde-fixed murine NIH-3T3 cells were carried out using an Olympus IX71 microscope equipped with a 60x 1.2 NA water immersion lens and a Becker&Hickl DCS-120 FLIM Scanner. Staining was done with 1 µM of Hoechst34580. Photon counting was performed over a period of 20s at 80 MHz laser repetition rate.

Results and Discussion

One of the hallmarks of fluorescence lifetime imaging is its independency on the non-quenched fluorescence intensity. Surprisingly, a fluorescence lifetime correlation to the recorded photon numbers became apparent in our FLIM measurements upon changing laser intensity. Loss of recorded photons is likely to occur due to the dead time of the FLIM detection (in the order of 100 ns) even at relatively low count rates in the order of 1 MHz [3]. In case of inhomogeneous samples, local count rates might exceed average values by far, leading to a decrease in intensity contrast (Fig 1a). At high counting rates exceeding 10% of the laser pulse rate of 80MHz the preferential detection of the first (early) photon gives rise to a loss of a potential second photon in the same signal period leading to a so-called pile-up effect. This yields a deformation of the excitation decay curve and in turn, results in an underestimation of the calculated lifetime.

As we faced high local count rates (6 MHz) due to bright areas in the detection field, we applied a pixel-wise mathematical correction of counting loss and pile-up (using the corrected incident photon rates up to 20 MHz). Figure 1 (a) and (b) show the impact of counting loss correction on the intensity images of ion-hit NIH 3T3 cells stained with 1 µM Hoechst34580. Fig. 1 (c) depicts the uncorrected lifetime image recorded at an average count rate of 2.7 MHz. An average lifetime correction of 2 % was calculated, but correction values of 3 % for bright areas were determined. The corresponding lifetime image with pile-up correction is shown in panel (d). Adopting the color LUT (insert) the compaction dependent lifetime as well as the radiation induced decompaction (insert) are still visible. Hence, our investigation proved that although pile-up effect affected the lifetime, the observed chromatin compaction dependent lifetime and radiation changes were not introduced by instrumental artifacts.

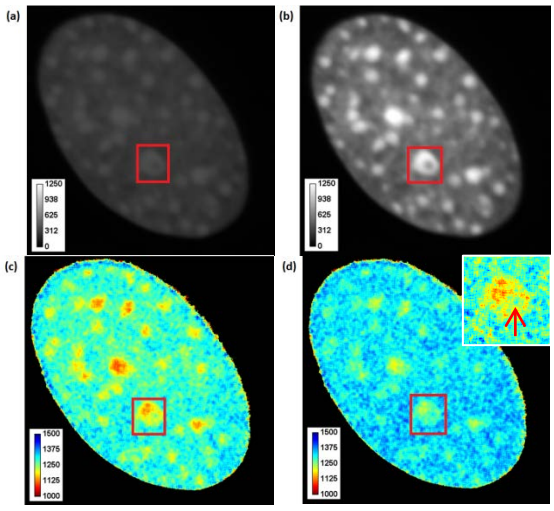

Figure 1: Confocal FLIM image of an irradiated NIH-3T3 cell nucleus stained with Hoechst 34580. Uncorrected (a, c [2]) and corrected (b, d) intensity and lifetime images. The ion-hit chromocenter is enclosed in the red rectangular and magnified with adjusted LUT in 1d. Arrow marks position of ion traversal.

References

[1] B. Jakob et al., NAR, 39, 6489-99 (2011).
[2] E. Abdollahi et al., NIMB. 365, 626-630 (2015).
[3] W. Becker, The bh TCSPC handbook 6th , 2014.

* This work is supported by the German federal ministry of education and research (BMBF), Grant#: 02NUK037A and DFG GRK1657.

DOI:10.15120/GR-2017-1

Imaging chromatin under near native conditions using transmission electron microscopy*

S. Tonnemacher[1], M. Eltsov[2], D.Grewe[2], A. Frangakis[2], G. Becker[1], G. Taucher-Scholz[1,3] and B. Jakob[1]

[1]GSI, Darmstadt, Germany; [2]BMLS, Frankfurt, Germany; [3]Technical Universität Darmstadt, Germany

Introduction

The resolution of optical microscopy has its limitation due to the diffraction barrier defined by the wavelength of the light. Besides recent approaches circumventing the diffraction barrier by a more precise determination of the signal origin, electron microscopy (EM) provides a traditional tool to obtain a much higher resolution. However structural modifications introduced by the chemical fixation methods needed for the preparation of biological samples are noticeable at this high resolution. To study radiation damage or other radiation induced changes in cells, it is necessary to develop and use fixation methods that largely preserve the structures of interest (i.e. chromatin) in a near native state. The method applied here for the future study of charged particle induced chromatin changes High-Pressure-Freezing (HPF) and subsequent Freeze-Substitution (FS) [1, 2].

Materials and Methods

NIH-3T3 cells were cultured on 3mm sapphire glasses coated with carbon at the GSI Target Lab glass was put in a flexiPrem (Sarstedt, Nürnberg) chamber in a petri dish (Fig.1a). HPF and all following steps were done at the BMLS in Frankfurt. The HPF was done with the Leica HM HPM100 in a sample cartridge (Fig.1b). FS with Lowicryl was done using a Leica EM AFS2.

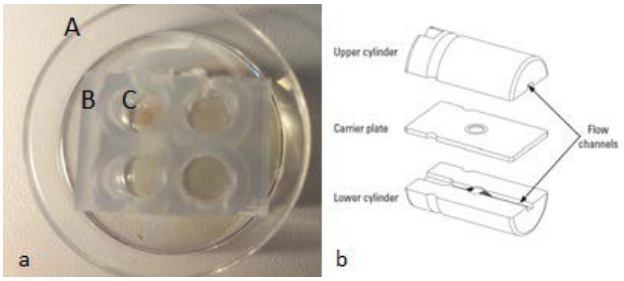

Figure 1: a) 35mm plastic petri dish (A) with a modified flexiPrem (B). Each chamber has a diameter of 5mm; inside each chamber is a 3mm sapphire (C). b) Sample cartridge for HPF consists of three parts. While freezing the sample is placed in the carrier plate (figure from [3]).

During HPF living cells are frozen rapidly to the temperature of liquid nitrogen while simultaneously exposed to a very high pressure of 2100bar within 20ms [1]. This procedure prevents the formation of ice crystals in wet biological samples and favours the formation of amorphous ice. The lack of crystalline ice and the absence of chemical fixation preserve internal structures much better than using other fixation methods. Following the HPF the frozen cells were immersed in acetone (containing 0.1% uranyl acetate (UA) to contrast membranes and nucleic acids) at -90°C for more than 24h to substitute the water molecules. After substitution, the samples were slowly warmed to room temperature while displacing the acetone by HM20, a Lowicryl resin. For imaging at a transmission EM (TEM) thin sections (200nm) were cut using an ultramicrotome and contrasted with uranyl acetate (UA) and lead citrate (LC).

Results

Using this HPF protocol, it is possible to image the cellular chromatin in a near native state. Due to the contrasting with UA and LC the chromatin was well visible and different stages of compaction (e.g. heterochromatin) could be observed. In addition nucleoli could be easily recognised (Fig. 2).

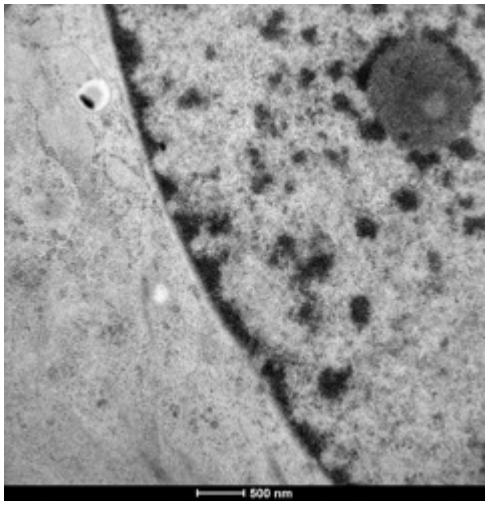

Figure 2: TEM image of a part from a NIH 3T3 cell. The nuclear membrane is visible in the middle of the figure; it goes from the top to the bottom. On the left side is the cytoplasm, on the right side the nucleoplasm with the heterochromatin (black structure) and the nucleoli (dark grey area on the top right). Section was cut, stained and imaged by Mikhail Eltsov.

Outlook

The quality of structural preservation and the obtained resolution might allow analysing radiation induced changes in the chromatin structure after irradiation with x-rays and ions.

References

[1] D. Studer et al., Histochem Cell Biol., 130, 877- 89 (2008)

[2] E. Johnson et al., Sci Rep, 5 (2015)

[3] Leica EMHPM100 Brochure

* This work was supported by BMBF Grant 02NUK037A and the graduate school HGS-HIRe.

Measurement of the time response of the beam monitors used for fast raster scanning

U. Weber[1], B. Voss[1], C. Schuy[1], K. Zink[2], C. Graeff[1]
[1]GSI, Darmstadt, Germany; [2]University of Applied Sciences Mittelhessen – THM (IMPS)

Speed improvement of the raster scanning is one of the most important prerequisites for the treatment of moving tumours such as lung or liver. One bottle neck in the existing raster scanning systems was turned out to be the gas filled beam monitors used for control of the scanning. Even when using fast amplifiers and fast data processing of the detectors, the relatively slow drifting time of the positive ions remains and significantly delays the signal. In this work we modelled and measured the time response of the integral parallel plate ionization chambers (PPIC) from the GSI pilot project [1]. They were tested with four different types of gas fillings: Ar/CO_2 (80%/20%), air, Helium, Nitrogen. The output signals from the PPICs were amplified using fast current amplifiers (Stanford-SR570m) and recorded via a fast storage oscilloscope. In order to measure the time response from a short beam pulse we used fast beam pulses (<3µs) from a 6 MeV Photon Linac or from the GSI synchrotron (^{12}C, 300 MeV/u) with fast extraction mode. The voltage of the detectors was varied from 100 to 2000 V.

The measured signals induced by the short beam pulses show a fast contribution from the fast drifting electrons and a much slower signal from the positive ions due to their much lower mobility [2].

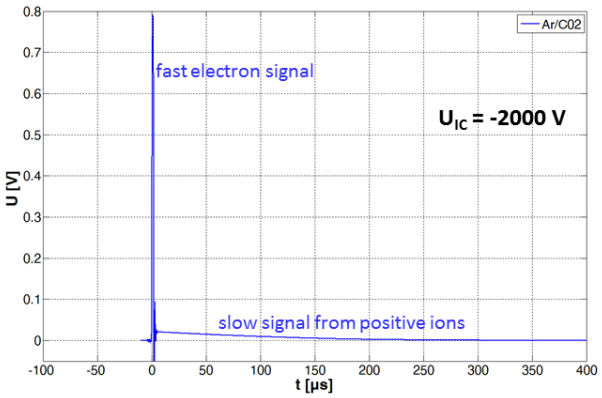

Figure 1: Measured time response of a parallel-plate ionization chamber filled with Ar/CO_2 for a short ion-beam pulse (^{12}C 300 MeV/u, <3µs). Shown is the signal at a voltage of 2000 V.

Furthermore, the type of gas has a strong influence on the response time. Especially, helium as detector gas strongly accelerates the time-response, because the mobility µ of helium ions is much higher compared to that of the other gases [2][3]. The time $t_{80\%}$ - until 80% of the charge is collected - is more than two times faster for Helium than for Ar/CO_2, air or Nitrogen (see figure 2). On the other hand, helium gas has the drawback, that due to its lower density the total signal is about 5-8 times smaller than for the other gases, which could result in higher noise, especially for low intensity beams (e.g. for scanning of proximal slices and/or for rescanning techniques).

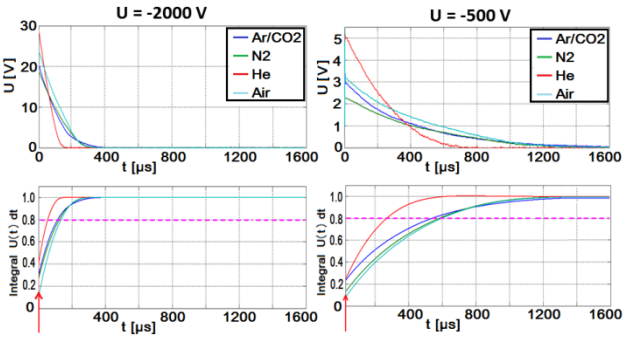

Figure 2: The upper diagram shows the pulse-answer signals for four different gases at voltages of 2000 V (left) and 500 V (right). The lower diagrams show the corresponding integrated signals normalized to 1. The $t_{80\%}$ values (intersection with dashed line) are useful parameters for the evaluation of the detector delay due to the ion drift time. The red arrow depicts the point in time of the beam pulse

We can conclude from figure 2 that the time response of the beam monitors can be dramatically improved by increasing the voltage. This requires a design of the ionization chambers which is resistant to high voltages [1]. A further improvement by a factor of two can be yielded by using helium gas. However, especially for low beam intensities, this requires a careful design of the amplifiers and good noise-shielding of the chambers.

References

[1] H. Stelzer, B. Voss , “Ionization chamber for ion beams and method for monitoring the intensity of an ion beam”, US patent, 6,437,513 B1, 2000.
[2] F. Sauli, “Principles of Operation of Multiwire Proportional and Drift Chambers”, 10.5170/CERN-1977-009, 1977.
[3] K. Kleinknecht: “Detectors for Particle Radiation”, Cambridge University Press, ISBN 0521640326, 1998.

DOI:10.15120/GR-2017-1

Nanoparticles radio-enhancement of ion beams at different oxygenation conditions*

M. Bolsa[1, #], D. Boscolo[2], E. Porcel[1], S. Lacombe[1], O. Sokol[2] , J. Wiedemann[2] , E. Scifoni[3], W. Tinganelli[3], B. Jakob[2], S. Roux[4], G. Jimenez[4], M. Durante[3] M. Kraemer[2]

[1]Institut des Sciences Moléculaires d'Orsay (UMR 8214) Bât 351, Université Paris Sud, CNRS, 91405 Orsay, France.
[2]Biophysics, GSI Helmholtzzentrum für Schwerionenforschung GmbH, Planckstr. 1, 64291 Darmstadt, Germany.
[3]Trento Institute for Fundamental Physics and Application (TIFPA-INFN), 38123, via Sommarive 14, Trento, Italy.
[4]Institut UTINAM, Université de Franche-Comté, CNRS, UMR6213, 25030 Besançon cedex, France.

Low oxygen concentration in cancer cells results in significantly lower cell death after exposure to ionizing radiation. It has been observed that heavy ion therapy under certain conditions would favour the treatment of hypoxic tumours as compared to conventional radiotherapy [1]. However, the irradiation of healthy tissues at the entrance channel remains a major limitation. A new strategy based on the combination of high-Z nanoparticles (NPs) with ion radiation has been developed by the group of S. Lacombe to improve the performance of heavy ion therapy [2, 3]. The addition of NPs increases the radiation effects within the tumour allowing ultimately the reduction of the dose deposited in healthy tissues. The group has studied the physico-chemical events that take place at nanoscale. In particular, it was shown that water radicals play a major role [3]. In the present work, the possibility of using AuNPs to increase radio-induced cell killing also in the case of hypoxia was addressed. The results of a series of experiments performed at HIT and GSI investigating the effect of AuNPs on HeLa (human cervical cancer) cells in oxic and anoxic conditions are presented in this report.

HeLa cells were gassed with a mixture of 95% N_2 and 5% CO_2 inside the exposure chamber 2 hours prior irradiation to achieve anoxic conditions (0% O_2). In oxic conditions, cells were kept in the exposure chamber but without gassing. Cells were incubated with AuNPs 6 h before gassing at a concentration of 1 mM in Au. At this concentration, AuNPs are not toxic. AuNPs, synthesized by S. Roux and co-workers, are composed of a gold core (2.5 nm) and encapsulated within an organic shell of DTDTPA [4]. Cells were irradiated with carbon ion beam at fixed <LET> (dose averaged linear energy transfer) values of 50 and 100 keV/µm. The combined effect of radiation and NPs on cells was quantified by the measurement of the mitotic survival, and by the quantification of radiation-induced nuclear DNA double strand breaks (DSB).

The surviving fraction of cells for <LET>=100 keV/µm can be reduced in the presence of AuNPs by 25% at 2 Gy in oxic and anoxic conditions and up to 45% at 4 Gy in anoxic (Figure 1). For <LET>=50 keV/µm, we did not find any NPs-induced radio-enhancement (NRE). We thus observed that the NRE seems to increase with LET. The nucleic DNA repair assay has demonstrated that AuNPs have no impact on DNA damage whatever the oxygenation condition without irradiation. However, the number of DSBs produced by radiation differs in between oxic and anoxic conditions in the absence of NPs but not in the presence of NPs (data not shown).

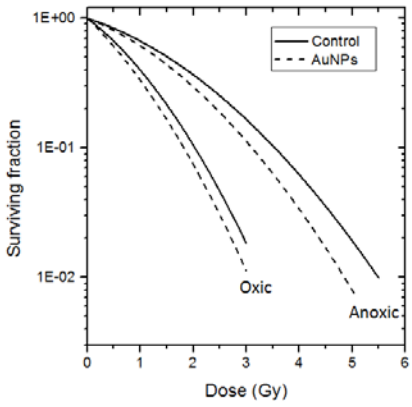

Figure 1: Surviving fraction of cells after irradiation by carbon ion beam (<LET> = 100keV/µm) versus the dose in oxic and anoxic conditions in presence or absence of AuNPs.

However, an exhaustive nanoscopic model able to describe the mechanism underlying the radio-induced effects of NPs and the role of oxygen concentration is still missing. For this reason both a Monte Carlo track structure and a LEM like model are in development in order to interpret these experimental results.

References

[1] Scifoni, E., et al. Phys Med Biol 58.11 (2013): 3871.
[2] Porcel, E., et al. 2014, Nanomedicine vol 10, Issue 8, p1601-1608
[3] Porcel, E., et al. Nanotechnology 2010; 21(8):85103.
[4] Debouttière, P-J., et al. Adv. Funct. Mater. 2006, 16, 2330-2339.

*The research leading to these results has received funding from the European Union Seventh Framework Programme [PEOPLE 2013 ITN ARGENT project] under grant agreement n [608163] and the BMBF Grant 02NUK037A.
marta.bolsa-ferruz@u-psud.fr

DOI:10.15120/GR-2017-1

Characterization of neurospheres generated from irradiated human embryonic stem cells*

M. Mayer[1], *O. Arrizabalaga*[2], *J. Kunz*[2], *S. Ritter*[2], *S. Sadeghi*[†2], *and C. Thielemann*[1]

[1]University of Applied Sciences, BioMEMS Lab, Aschaffenburg, Germany; [2]GSI, Biophysics, Darmstadt, Germany

Cognitive dysfunctions as well as malformations of the brain have been observed after *in utero* exposure to ionizing radiation (IR) [e.g. 1]. Further, *in vitro* studies reported on altered neuronal and synaptic excitability induced by IR [2]. Therefore an assessment of radiation-effects on the developing central nervous system, especially on the electrophysiological properties, is needed. To address this topic we chose human embryonic stem cell (ESC)-derived neural stem cells as a model system. For further proliferation and differentiation neural stem cells (NSC) were grown as three-dimensional aggregates (neurospheres, NS) [3].

To characterize the formed NS, quantitative RT-PCR was performed demonstrating the expression of NSC markers NES, PAX6 and SOX2, as well as markers of neuronal progenitors such as DCX, MAP2, NR2F2 and TJP1, among others (data not shown).

To study the effect of IR on neural development, human ESC were irradiated with 1 Gy X-rays (250 kV, 16 mA). Controls were sham-irradiated. Four days later neural differentiation was initiated.

The proliferative capacity of the stem cells that form the sphere is reflected in the diameter. Previous studies on mouse ESC reported on a reduced diameter of spheres generated from irradiated cells [4]. To evaluate if NS derived from irradiated human ESC show an altered diameter compared to the control, the area of the NS was determined from microscopic images (Nikon Eclipse, TS100) using the NIS-Elements Documentation software™ (Fig. 1a).

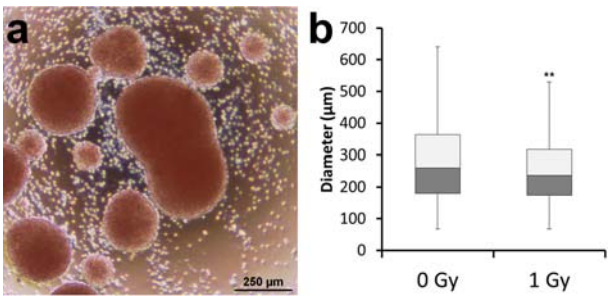

Figure 1: Diameter of NS. (a) An exemplarily image of NS 14 days after formation. NIS-Elements Documentation software™ was used to measure the area and automatically calculate the diameter. (Scale bar = 250 μm) (b) Boxplot showing NS diameter in quartiles, whiskers show minimum and maximum values (after discarding the outliers, which were calculated by "Outlier = Q3 + 1.5 x interquartile range") (n= 413 for 0 Gy, n= 257 for 1 Gy, ** $P < 0.01$).

* Funding for this project was provided by the Federal Ministry of Education and Research (02NUK025C and 02NUK034C).

† S. Sadeghi received funding from "Verein für Tumortherapie".

The mean diameter of NS originated from irradiated human ESC was smaller than the respective control, i.e. 251 +/- 97 μm compared to 274 +/- 119 μm. As displayed in Fig. 1b, the quartile-distribution of the diameters also showed a statistically significant difference between sham and 1 Gy irradiated samples.

To evaluate if irradiated human ESC-derived NS are electrically active, we used microelectrode arrays (MEAs) as previously described [3]. NS within the interquartile range size were placed onto MEA chips. Electrophysiological recording started 1 day after plating. The results clearly showed that irradiated human ESC are still able to form electrophysiologically active NS. Noteworthy in both groups a comparable number of spikes per minute (365,6 +/- 130,92 for 0 Gy, 438,2 +/- 178,45 for 1 Gy) was recorded on day 1 of electrical activity (Fig. 2). On day seven the number of spikes increased about threefold in sham irradiated samples, while the amount of signals in NS derived from irradiated human ESC increased only by a factor of 1,42 +/- 0,5. These preliminary data indicate that exposure of human ESC to IR affects the electrophysiological properties of their progeny.

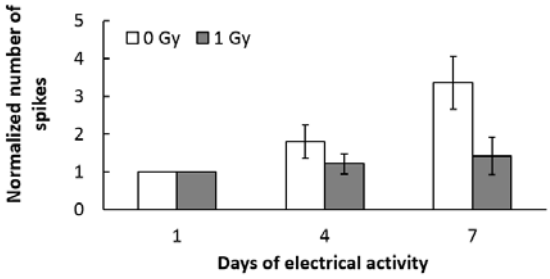

Figure 2: Number of spikes recorded from single NS. NS derived from 0 Gy or 1 Gy X-ray irradiated human ESC were cultured on MEAs. The number of spikes was examined for 60 seconds on day 1, 4 and 7 of electrical activity. Data are represented as mean normalized to day 1 (n = 5 for 0 Gy, n = 5 for 1 Gy) +/- SEM.

Currently, further electrical recordings of NS are being generated and analyzed to validate the data obtained so far. Moreover, gene expression studies are being carried out, in order to determine the cellular and molecular composition of the NS. The exposure of human ESC to IR could influence their differentiation capability, i.e. forming non-functional neurons or other types of neural cells.

References

[1] Verreet, T. et al., JNeurodevDisord. 2015, 7: p. 17-21
[2] Ordy, J.M. et al., JNeurochem. 1968, 15: p. 1245-1256
[3] Mayer, M. et al., GSI Scientific Report 2015, p. 205
[4] Helm, A. et al., Stem Cells Dev. 2016, 25:p. 178-188

DOI:10.15120/GR-2017-1

Semi-automatic analysis of dicentric chromosomes for cytogenetic risk assessment of low radiation doses*

C. Hartel[1], *Y. Knies*[1] *and S. Ritter*[1]
[1]GSI, Darmstadt, Germany.

In the context of the GREWIS project, we aim to determine the cytogenetic risk associated with the therapeutic exposure to very low doses of (densely or sparsely) ionizing radiation. The scoring of dicentric chromosomes (DCs) is a standard technique for biological dosimetry and the assessment of genotoxic risk [1]. To determine the cytogenetically equivalent dose, the frequency of DCs in a sample of peripheral blood lymphocytes is compared to a reference dose-effect curve. DCs can be scored manually; yet, to achieve an adequate resolution in the low-dose range, analysing a high number of metaphases is essential. Therefore, a software-based image acquisition and a semi-automatic analysis system was established in our laboratory and a dose-effect curve was generated.

Irradiation and chromosome preparation were performed as described previously [2]. Briefly, peripheral blood lymphocytes were exposed *in vitro* to X-rays (dose range 0-6 Gy). Metaphase spreads were prepared and were stained with Giemsa dye. DC scoring was performed using an Axio Imager Z2 microscope (Zeiss, Germany) and the DCScore/Metafer software (Metasystems, Germany). The automatically detected DCs were reviewed by an experienced scientist and false positives were removed. We accept as true positive DCs only those which clearly have the typical shape and are accompanied by an acentric fragment. Examples of a true DC as well as a false positive DC are shown in figure 1. In the unexposed control, the vast majority (98.5%) of all automatically detected DCs are false-positives, this value drops to 11.9 % of false positives at a dose of 4 Gy. This is in good agreement with literature data [3].

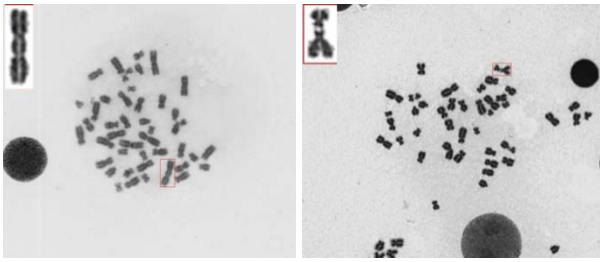

Figure 1: Left: Metaphase with a true DC, the acentric fragment is also visible in the metaphase spread. Right: Metaphase with a false positive DC, two aligned chromosomes are scored by the software as one DC.

The resulting dose effect curve for the *in vitro* induction of DCs in peripheral blood lymphocytes is shown in figure 2. We observed 0.103±0.017 DCs per 100 analysed metaphases in the unexposed control and 0.156±0.020 in the sample exposed to the lowest dose of 25 mGy (each based on 35 000 analysed metaphases), showing that the exposure to a dose of 25 mGy can be distinguished from the background level. For higher doses, a lower number of analysed metaphases was sufficient. The calibration curve constructed so far is based on 100 000 analysed metaphases (figure 2).

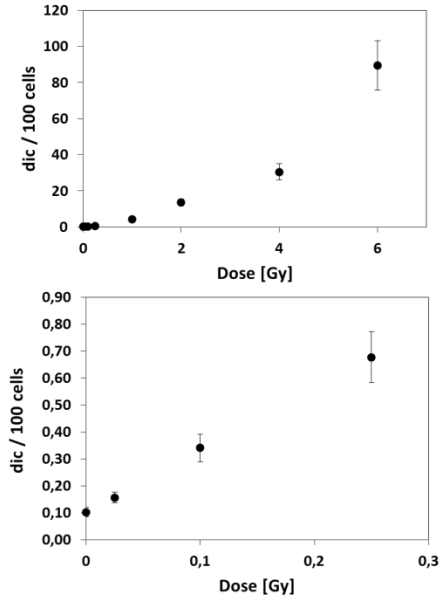

Figure 2: Dose-effect curve for the induction of DCs by X-rays in peripheral blood lymphocytes. The low-dose range (0-0.25 Gy) is shown in the lower panel.

The analysis of DCs is currently used to determine the cytogenetic effect of *in vitro* exposure to radon gas on lymphocytes. Furthermore, we will apply the semi-automatic scoring of DCs to assess the cytogenetic risk of the therapeutic exposure to low doses of sparsely (low dose radiotherapy, LDRT) or densely (radon therapy) ionizing radiation *in vivo*.

References

[1] IAEA Technical Report Series No 105: Cytogenetic Analysis for Radiation dose Assessment. International Atomic Energy Agency 2001.

[2] Lee *et al.* Chromosome aberration measurements in mitotic and G2-PCC lymphocytes at the standard sampling time of 48 h underestimate the effectiveness of high-LET particles. Radiat Environ Biophys 50 (2011) p371-381.

[3] H. Romm *et al.* Automatic scoring of dicentric chromosomes as a tool in large scale radiation accidents. Mutat Res 756 (2013) p174-183.

* Work supported by the Federal Ministry of Education and Research (Bonn, Germany) under contract number 02NUK017A.

Pharmacological augmentation of heavy ion cancer therapy *

Norman Reppingen[1], *Marco Durante*[2], *and Claudia Fournier*[1]

[1]GSI Helmholtzzentrum für Schwerionenforschung; [2]Trento Institute for Fundamental Physics and Applications - TIFPA

Our ongoing *in vitro* efforts (see previous reports)[1] aim to find a most versatile pharmacological augmentation of heavy ion cancer therapy. Recently, we evaluated a multimodal pharmacological approach in the murine cell lines CT26.WT, B16-F10 and 4T1. Using the 4T1 cells (metastatic breast cancer), we extended this evaluation to a mouse model with and without x-ray irradiation. One of the pharmacological entities did demonstrate impressive efficacy with strongly reduced tumor growth. This reveals our model of choice as a potentially useful test system to demonstrate the versatility of heavy ion cancer therapy.

In vitro progress

In the CT26.WT cells (colon carcinoma) and in the B16-F10 cells (melanoma) we were able to induce apoptotic cell death also in conjunction with irradiation. The evaluation of our approach with the 4T1 cell line was reflecting the known high treatment resistance of this model. We were able to show the activity of a tyrosine kinase inhibitor to at least partly antagonize this treatment resistance, inducing tumor cell death. These in *in vitro* results, although encouraging, were limited by the absence of an immune system and tumor stroma, which is known to influence tumor *in vivo* behavior and to contribute heavily to treatment resistance.

In vivo results

To gain more insights on immunological mechanisms and to validate overall efficacy, we evaluated our pharmacological approach in an immune competent mouse model with 14 Gy of x-ray irradiation confined to the tumor. Irradiation with x-ray alone led to a minor reduction in tumor growth (see figure 1). The tyrosine kinase inhibitor reduced tumor growth efficiently. The tumor shrinkage took place without any signs of toxicity under close monitoring of health status and individual mouse weight. As the remaining tumors were small but visible, there still remains room for improvement to evaluate the versatility of heavy ion cancer therapy in this particular and potentially other combined applications.

* Work supported by HGShire. In vivo animal work was carried out by TRON GmbH.

Outlook

One of the next steps is to find new interesting drug candidates. Also, we need to gain deeper insights into cell death mechanisms, as e.g. 4T1 cells are p53 negative and -as many other cancer cell types- unlikely to succumb to apoptosis. Histological analysis of the experimental specimens gained from the animal experiments will hopefully hint to further pharmacological optimization strategies to maximize carbon ion cancer therapy efficacy. As we have reasons to assume that carbon ion irradiation could lead to a more pronounced decrease in tumor growth, a further validation of a combined regimen including heavy ions is one of the upcoming aims.

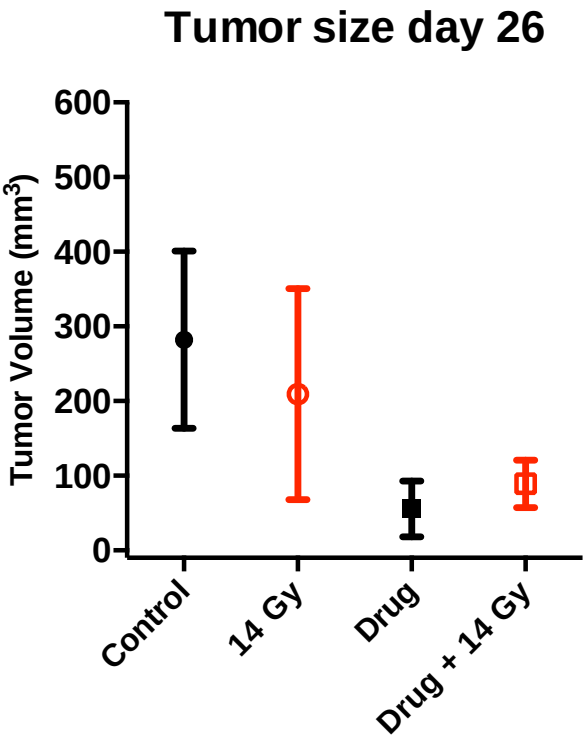

Figure 1: Representative tumor sizes (sample groups between 7 and 13 animals) with drug treatment beginning at day 5 and 14 Gy of x-ray irradiation (tumor) at day 14.

References

[1] N. Reppingen, M. Durante, C. Fournier, Scientific Reports 2014

DOI:10.15120/GR-2017-1

Comparison of relative biological effectiveness of proton radiation for regeneration of intestinal crypts in mice with the Local Effect Model*

R. Grün[1], T. Friedrich[1], M. Krämer[1] and M. Scholz[1]
[1]GSI, Darmstadt, Germany

Introduction

The role of relative biological effectiveness (RBE) consideration in proton radiotherapy different from the dogma of a constant RBE is gaining interest for clinical application. In a previous report [2], we were comparing proton RBE predictions by the Local Effect Model (LEM) [1] to experimental RBE values for clonogenic cell survival (*in-vitro* data). To further demonstrate the capabilities and limitations of LEM for proton irradiation along the spread out Bragg peak, here we focus now on the comparison to experimental *in-vivo* data. The endpoint intestinal crypt regeneration in mice after single fractions of proton irradiation was chosen since the intestinal crypt assay is an established and widely studied endpoint with a sufficient amount of data available in the literature.

Methods

Ten *in-vivo* experiments for the survival of intestinal crypts in mice were considered for the comparison. We compared the RBE for 10 and 20 surviving crypts to the RBE prediction by the LEM in dependence on dose-mean linear energy transfer (LET_D). The treatment planning software TRiP98 was used to optimize the passive proton SOBP of each experiment. For the comparison with *in-vivo* data, mainly single fraction experiments with high doses exceeding 10 Gy were examined. The LEM is based on the so-called single particle approximation (SPA), which is expected to show limitations for high doses. Therefore, we additionally used the so-called 'full simulation' version (FS) of the LEM for the comparison to account for the potential limitations of the SPA at higher doses [3]. More detailed information about the analysis can be found in [4].

Results & Conclusion

The RBE values predicted by the LEM (SPA) were evaluated using the photon dose given in the publications, which leads to 10 and 20 surviving crypts, respectively. A systematic shift to lower RBE values for the LEM (SPA) and LEM (FS) prediction as compared to the experimental RBE is observed (fig. 1). The deviation of the RBE values for 10 surviving crypts is of the order of 5% for LEM (SPA) and 2.5% for LEM (FS). For 20 surviving crypts the deviations are only slightly higher. The constant underestimation was attributed to the high doses of around 13–16 Gy needed to study this endpoint. Regarding the 95% confidence interval, the LEM (FS) prediction as well as a constant RBE of 1.1 seem to be in good agreement with the experiments. Nevertheless, the trend of an increasing RBE with increasing LET_D as observed in the experiments is better described by the predictions of both LEM (SPA) and LEM (FS).

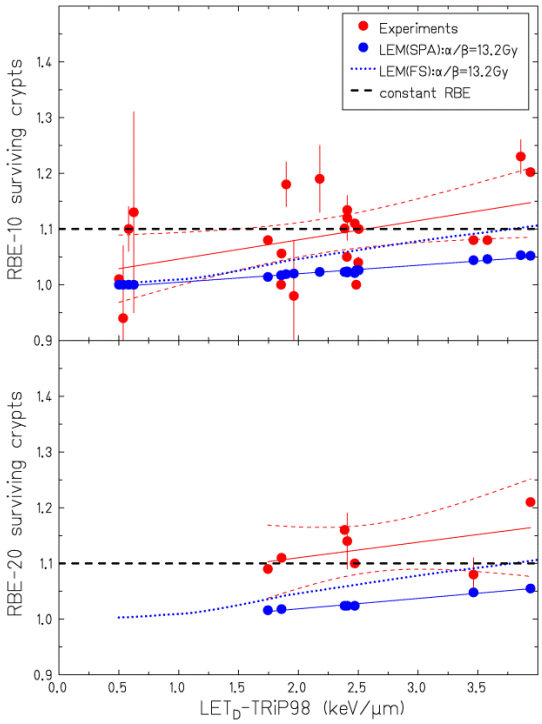

Figure 1: RBE vs. LET_D for 10 and 20 surviving intestinal crypts in mice. The blue data points and solid blue line (fit curve) correspond to the LEM prediction with the SPA. The red line represents a fit to the experimental values (red circles). Note that for the fit no error bars were considered. Thin red dashed lines show the 95% confidence interval for the experimental values. For the LEM predictions the 95% confidence interval coincides with the fitted curve (solid blue line).

References

[1] T. Elsässer et al., Int J Radiat Onc Biol Phys (2010)
[2] R. Grün et al., GSI Scientific Report 2015 (2016)
[3] Friedrich et al., Int J Radiat Biol (2012)
[4] R.Grün et al., Phys Med Biol (2017)

* Work supported by RaySearch Laboratories AB

Influence of ionising radiation on the capacity of neural stem cells to form neurospheres*

O. Arrizabalaga[1], L. Muñoz-Rizzo[1], D. Ney[1] and S. Ritter[1].
[1]GSI, Darmstadt, Germany

Human embryonic stem cell derived neural stem cells (hNSC) are a powerful model system to study the effects of ionizing radiation (IR) on neurogenesis [1], a fundamental part of brain development and homeostasis. The method of choice to determine the ability of a cell to survive radiation exposure is the colony forming assay that measures the ability of a single cell to form a colony in a culture dish. Yet, colonies cannot be grown from single hNSC in adherent culture. An alternative approach is the cultivation of NSC in suspension as 3-dimensional aggregates, called neurospheres (NS).

As culture dish and cell density are critical parameters that influence the NS formation efficiency, we optimized the technique for two types of suspension culture vessels, i.e. T25 flasks and 96-well round-bottom plates. In T25 a larger number of NS can be grown (e.g. for further molecular biological analyses), whereas in microplates a single NS can be grown per well. First, different seeding densities were tested from 100 cells/µl down to 1 cell/µl. These experiments showed that an appreciable number of NS with a comparable size is generated by seeding 5 cells/µl in T25 flasks, while a seeding density of 1 cell/µl for 96-well plates results in one single NS per well.

NS were allowed to grow for 2 weeks, and then their number and size (diameter) was determined. NS formed in T25 flasks were analysed using an in-house developed automatic counter recognizing objects greater than 35 µm [2], while NS grown in 96-well plates were analysed using a Nikon Eclipse TS100 microscope and the NIS Elements Documentation software™.

Having established these techniques, a first radiation experiment was performed. hNSC were exposed to 1 or 2 Gy X-rays (250 kV, 16 mA) and seeded 1 or 2 days after exposure for NS formation. Analyses of NS number and size were performed 14 days later (Figure 1).

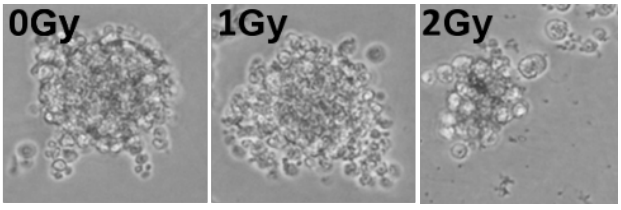

Figure 1: Representative images of NS generated from X-ray irradiated hNSC in 96-well plates. NS formation was initiated 1 day after exposure.

As shown in Figure 2, in each experimental set up the NS formation capacity of irradiated NSC was found to be affected by dose and post-irradiation incubation time. Yet, the data obtained for NS grown in T25 flasks shows a higher inter-experimental variability.

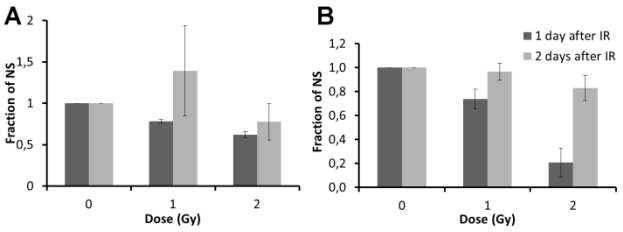

Figure 2: Fraction of NS formed in T25 flasks (**A**, n = 2) or 96 well plates (**B**, n = 7). Cells were seeded 1 or 2 days after X-ray exposure. Data was normalized to the sham irradiated control (mean ± SD).

Noteworthy, in control samples the diameter of NS grown in T25 flasks was 54 ± 7 µm and was not significantly affected by radiation (Figure 3 A). On the other hand, the diameter of control NS formed in 96 well plates was larger (91 ± 13 µm). Irradiation of hNSC with X-rays resulted in slightly smaller NS compared to the control. This effect showed a dose-dependency, but no substantial difference was observed between NS formation 1 or 2 days after X-ray exposure (Figure 3 B).

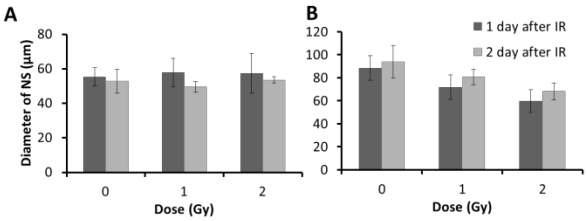

Figure 3: Mean diameter of NS (± SD) generated in T25 flasks (**A**) or 96-well plates (**B**). Cells were seeded 1 or 2 days after X-ray exposure.

In summary, our data show that the neurosphere formation assay can be applied for assessing the effects of IR on hNSC, resembling the classical colony forming assay for adherent cells. Moreover, our results suggest that 96-well plates possess a number of advantages in comparison with T25 flasks, e.g. the inter-experimental variation in the NS formation efficiency is lower. If this is due to the fact that in each well only one sphere is formed and thus fusion and aggregation of NS cannot take place remains to be elucidated.

References

[1] Arrizabalaga et al., GSI Report 2016-1, p. 201
[2] Sonnemann et al., GSI Report 2014-1, p. 43

* Funding for this project was provided by the Federal Ministry of Education and Research (02NUK034C) and Verein für Tumortherapie.

DOI:10.15120/GR-2017-1

Cluster analysis of ionization patterns after ionizing radiation*

J. Renner[1], *M.Scholz*[1], *T. Friedrich*[1]
[1]GSI, Darmstadt, Germany

One determinant for the enhanced biologic effectiveness of ion radiation is the concentrated accumulation of ionization events delivered to the tissue. Ionization clusters facilitate the promoted induction of double strand breaks and possibly more severe lesions to the DNA. The Ripley J function provides a convenient tool to compare cluster properties of such ionization patterns of different radiation qualities, which is of relevance for biophysical models like the Local Effect Model (LEM).

The LEM is used to predict the biologic effectiveness of ion radiation for therapy in its original version. Its latest improved version (LEM IV) is now used for research purposes at GSI. It assumes that in any subvolume of cell nuclei covered by the track structure of ions as many double strand breaks (DSB) are induced to the DNA as if the local dose in that subvolume was deposited by high energetic photon radiation, for which the DSB yield is known. The notion of local dose is here based on an amorphous track description and falls off with the radial distance to the ion path. This approach does not explicitly consider the point like nature of radiation induced ionization sites. As the DSB is a consequence of clustering of at least two ionizations on opposite DNA strands within the spatial scale of a few nm, the amorphous track structure approach in LEM therefore requires that on this scale the clustering properties of ionizations in ion tracks and high energy photon radiation fields are comparable. While assessed by performance, reliability and robustness the LEM is validated in numerous ways, a full theoretic consideration of this assumption has not been attempted so far.

For a theoretic analysis of ionization patterns which can be obtained by Monte Carlo transport calculations, a method to characterize the clustering properties of an arbitrary ionization pattern (or, more abstract, point process) is needed. A formalism derived in ecology by Ripley allows quantifying the number of observed points in a given area in comparison to a complete random distribution of points [1]. This formalism was modified to three dimensions and adapted for describing ionization patterns. The quantity

$$J(L) = \sqrt[3]{\langle n \rangle - \rho_e L^3}$$

can be calculated for any ionization point pattern, where ρ_e is the overall density of points in the simulation volume, and $<n>$ is the average number of additional points within small cubic volumes of length L, centred around an arbitrary point. Hence J directly parameterizes the number of points exceeding the expected number by a random homogeneous distribution within the entire simulation volume. If the point pattern is free of any spatial correlation, no clustering is visible and $J(L) = 0$ for all L. Instead, if ionization points are clustered, e.g. as on secondary electron tracks ionizations occur in an organized way (like 'pearls on a string'), then clustering is visible as accumulation of ionizations along these tracks, leaving space in between tracks. In this case J is larger than 0 and rises with L, eventually getting constant when entire clusters are covered by the cubes of site length L.

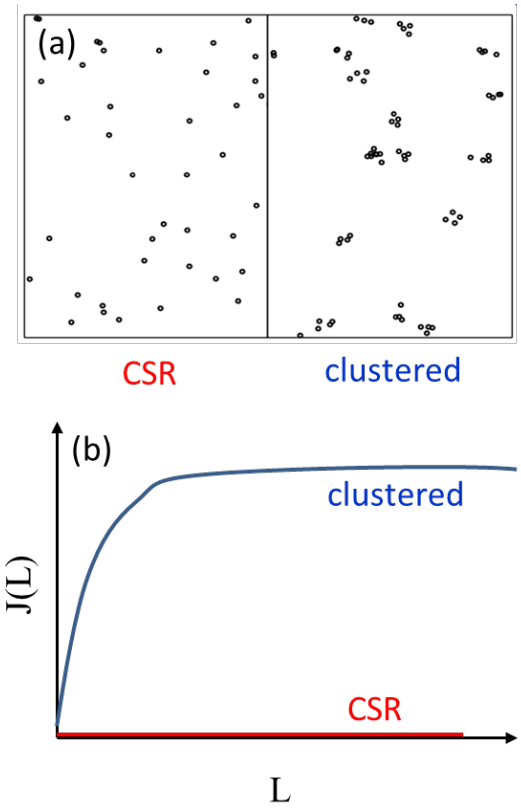

Figure 1: (a) Schematic 2D sketch of a point pattern following complete spatial randomness (CSR, left) and showing cluster agglomeration (right). (b) Ripley's J function allows a distinction between these cases for every probe size L.

On the relevant size for DSB induction of a few nm the function $J(L)$ can now be used to determine the degree of clustering in comparison to CSR for any radial distance to the ion path within its track structure formed by δ-electrons, and for high energetic photon radiation fields of equal dose. While a broader investigation is planned, first results at selected situations indicate a general similarity of the cluster properties of these cases.

References

[1] A.J. Baddeley and B.W. Silverman, Biometrics **40**, 1089 (1984).

DOI:10.15120/GR-2017-1

Nanodosimetry with quantum dots: Proton track structure simulations

M. Borghesi[*1], *M. Dapor*[1,2], *M. Krämer*[3], *I. Abril*[4], *R. Garcia-Molina*[5], *A. Quaranta*[6], *M. Durante*[1], *and E. Scifoni*[1]

[1]TIFPA, Trento, Italy; [2]ECT*, Trento, Italy; [3]GSI, Darmstadt, Germany; [4]Universitat d'Alacant, Spain; [5]Universidad de Murcia, Spain; [6]Università di Trento, Italy

Introduction

Ion beam nanodosimetry is an emerging method for radiation field characterization in particle therapy. Such a different dosimetry cannot substitute the standard methods, but is necessary to deal with as small volumes as DNA convolutions. Different phenomena must be taken into account at the nanoscale than those studied on a macroscopic level.

Dealing with these small volumes is very difficult on the experimental level. Several apparatuses have been built, e.g. [1], to measure the number of ionizations inside tissue-proportional gas chambers, which gave very good results (see e.g. [2]). However, such apparatuses are too large and lack of portability. As a consequence, new nanoscopic dose-measuring devices are needed for the evaluation of nanodoses. Recently [3], in the context of INFN experiment NADIR, quantum dots have been proposed as an alternative nanometric ionization-counting device due to their luminescence properties [4].

We performed a track structure analysis to characterize proton induced ionizations in these systems through the GSI code *TRAX* [5].

Cross section assessment

Two ionization cross section models have been compared: the binary encounter approximation or BEA, already implemented into the code *TRAX*, which only accounts for two-body collisions, thus neglecting all solid state interactions between target atoms; the dielectric response formalism, which includes empirical solid state effects by construction from optical limit measurements, extended to $k \neq 0$ regime via the Mermin model [6] which will be called MELF, i.e. Mermin energy loss function.

A comparison between these two models is depicted in figure 1, where every single differential cross section (SDCS) for proton projectile at kinetic energy $T = 1$ MeV is shown. The difference is restricted to low secondary electron energy $W < 20$ eV, while at higher energy the two curves almost perfectly overlap.

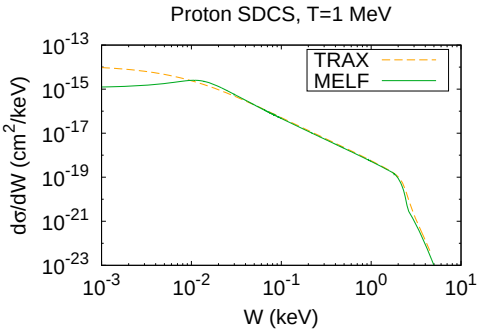

Figure 1: Ionization cross sections for 1 MeV proton on amorphous carbon, accounting (MELF) or not (BEA, labeled *TRAX*) for solid state effects.

Quantum dot nanodosimetry

When evaluating the number of ionizations produced inside an aC-dot, two components should be taken into account: the ionizations produced by direct traversal of the dot and those produced when ions pass aside the dot.

For what regards the former case, which turns out to produce many more ionizations, making the other one negligible, the number of ionizations is plotted in figure 2.

Such analysis served as a basis to design experimental conditions for aC-dot irradiation tests [7].

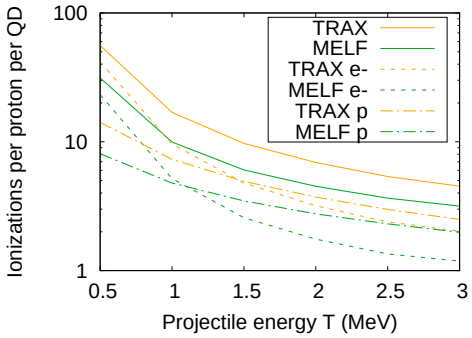

Figure 2: Ionizations produced by direct traversal of an aC-dot as a function of ion energy. Solid, dashed and dash-dotted lines represent respectively total, secondary electron and primary (i.e. ion induced) ionizations.

References

[1] Pszona S. *et al*, *Nucl. Instrum. Methods A*, 447(2000)601-607
[2] Conte V. *et al.*, *New Journal of Physics*, 14(2012)093010
[3] Pancheri L. *et al.*, *Radiother. Oncol.*, 118(2016)S88
[4] Kelarakis A., *MRS Energy & Sustainability*, 1(2014)E2
[5] Krämer M. & Durante M., *Eur. Phys. J. D*, 60(2010)195–202.
[6] Heredia-Avalos S. *et al.*, *Phys. Rev. A*, 72(2005)052902
[7] Borghesi M., *Master thesis*, University of Trento (2017)

*mauro.borghesi@tifpa.infn.it

DOI:10.15120/GR-2017-1

Space shielding simulations with TRiP98 for the ROSSINI-2 project*

M. Krämer[1#], E. Scifoni[2], M. Giraudo[3] and M. Durante[2]
[1]GSI, Darmstadt, Germany; [2]TIFPA-INFN, Trento, Italy; [3] Thales Alenia Space, Turin, Italy.

Introduction: a Space-TRiP?

The possibility of using TRiP98, the GSI in-house treatment planning system for particles [1] also for space radiation protection studies was already mentioned and discussed in a publication several years ago [2]. This was because his fully modular structure, and extensibility towards different regions of validity, e.g. of nuclear interaction cross sections. Here for the first time we realize modifications of the code dedicated to this purpose and perform several test of radiation shielding with different monochromatic and spectral particle radiation sources, in the context of the ESA ROSSINI-2 project[3].

Simulation tests

A series of tests were performed by modifying the internal transport code of TRiP98, normally used for beam model generation in particle therapy, extending it for handling different materials, and compound multi-layers of them. The shielding simulations were thus carried on with a numerical pencil beam monodimensional transport model. The same experimental setup described in the dedicated ROSSINI-2[3] technical notes, for the Monte Carlo transport codes (GEANT4 and PHITS), have been simulated. i.e., for the particle spectra a couple of ionization chambers were simulated before and after a layer of varying thickness of material. The complete setup was simulated packed, i.e., no air between the different layers of material.
Results have been presented for 2 different SPE proton spectra (ESP and "worst hour", August 72 (Aug72)) as well as for the carbon beam measured at HIT (430.1 MeV/u) by the GSI team [3].

Summary and Outlook

With these initial results, we show that TRiP98 may be efficiently used for dose reduction analysis in different materials, even if further efforts will be needed for a closer reproduction of the experimental data. A high energy extension of the transport code, i.e. in the GeV region, allowing description of GCR scenarios, is one of the next steps to take.

Material	*Aeric density (g/cm²)*	*Absolute depth (mm)*	*DR (%) (TRiP98)*	*DR (%) (Exp)*	*DR/masss (%/(g/cm2)) (TriP98)*
No target	0	0	100	100	
Water	3.49	35	95.0	97.74	1.43
PMMA	3.57	30	94.7	97.42	1.48
LiH	0.58	11	98.0	99.05	3.44
"	2.33	44	93.2	96.03	2.91
"	5.82	110	85.0	90.65	2.57
Alu2024	0.56	2	99.3	99.99	1.25
"	2.82	11	97.0	99.78	1.06
"	8.47	32	93.0	99.13	0.82

Table 1: Dose reduction (DR) for a carbon ion beam at 430.1 MeV/u with different shielding materials obtained with TRiP98 and compared to HIT experiments [3]

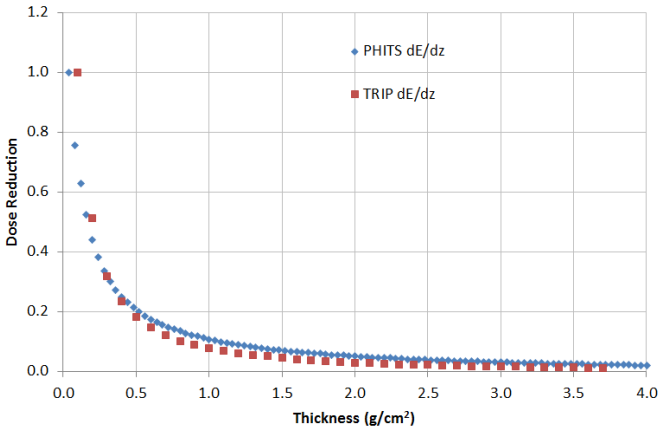

Figure 1: Comparison of depth dose profile of the Aug72 proton Spectrum in water as computed by TRiP98 and PHITS.

References

[1] M. Krämer and M. Durante, Ion beam transport calculations and treatment plans in particle therapy, Eur. Phys. J. D **60**, 195 (2010).
[2] M. Krämer, TRiP98 (TReatment PlannIng for Particles), THREE - Heal. Risk Extraterr. Explor. 2012, 1 (2012).
[3] U. Weber et al., Dose attenuation measurements in the ROSSINI-2 project for space research, GSI Sci-Rep 2016-1, Biophysics-46, p. 234 (2014).

* ROSSINI-2 is supported by ESA (Contr. No.4000112525/14/NL/LF)

#m.kraemer@gsi.de

DOI:10.15120/GR-2017-1